View metadata, citation and similar papers at core.ac.uk

brought to you by CORE

provided by NASA Technical Reports Server

NV-80
83154
P-43

NASA Technical Memorandum 4370

Variable-Camber Systems Integration and Operational Performance of the AFTI/F-111 Mission Adaptive Wing

John W. Smith, Wilton P. Lock,
and Gordon A. Payne

APRIL 1992

CSCL 01C Unclas
H1/08 0034194

NASA Technical Memorandum 4370

Variable-Camber Systems Integration and Operational Performance of the AFTI/F-111 Mission Adaptive Wing

John W. Smith
PRC, Inc.
Edwards, California

Wilton P. Lock and Gordon A. Payne
Dryden Flight Research Facility
Edwards, California

NASA
National Aeronautics and
Space Administration
Office of Management
Scientific and Technical
Information Program
1992

CONTENTS

PRECEDING PAGE BLANK NOT FILMED

PAGE INTENTIONALLY BLANK

LIST OF TABLES

LIST OF FIGURES

ABSTRACT

The advanced fighter technology integration, the AFTI/F-111 aircraft, is a preproduction F-111A testbed research airplane that was fitted with a smooth variable-camber mission adaptive wing. The camber was positioned and controlled by flexing the upper skins through rotary actuators and linkages driven by power drive units. This report describes the wing camber and control systems. The measured servoactuator frequency responses are presented along with analytical predictions derived from the integrated characteristics of the control elements. A mission adaptive wing system chronology is used to illustrate and assess the reliability and dependability of the servoactuator systems during 1524 hours of ground tests and 145 hours of flight tests.

INTRODUCTION

Modern tactical aircraft (A/C) must perform over a broad operational envelope. A common and practical method for optimizing the wing at any one flight condition, such as speed and altitude, loading, minimum fuel consumption, or maximum range, is to adjust both wing sweep and camber to a predetermined favorable value for that condition. On the other hand, maneuvers performed at nonoptimum flight conditions may result in an overall penalty. A desirable innovation could continuously vary the wing geometry, particularly camber, as a function of a measured flight parameter or as an integrated set of measured flight parameters. From feasibility studies and aircraft availability, the F-111A, used for the transonic aircraft technology (TACT) program, was selected as the logical aircraft for modifiying and developing a mission adaptive wing (MAW). A comprehensive discussion of the TACT/F-111 flight test results is given in reference 1. The resulting or new program, employing the variable-camber concept, was designated as the advanced fighter technology integration (AFTI/F-111) aircraft.

The objectives and goals of the AFTI/F-111 program were to design, implement, and explore the technology of a smooth, variable-camber wing. The MAW design incorporated flexible fiberglass skins on the upper leading edge (LE) and trailing edge (TE). This design enables the upper surfaces, when flexed cordwise, to have a smooth, continuous contour (fig. 1). To affect the complete sectional distortion, the area along the bottom surfaces near the LE and TE was reduced by using sliding panels overlapping to give minimal discontinuity along the spanwise seams. The controlled camber curvature was obtained by a cascade of internal mechanisms composed of hydraulic power drive units (PDU's), rotary actuators, and mechanical linkages. These mechanisms deformed the wing downward starting at the hinge line. There were eight individually controllable segments, two on the LE's and six on the TE's. Primary control was commanded and accomplished through a dual-redundant, fly-by-wire, digitally programmed flight control system. A dual-redundant analog system provided manual backup control. A description of the software, hardware, and redundancy management systems is reported in reference 2.

The AFTI/F-111 program was divided into two phases. Phase 1 addressed design and construction of the manual flight control system (MFCS) and extended through part of the flight testing up to the implementation of the automodes. The phase 2 ground and flight testing addressed integration and implementation of the automatic flight control system (AFCS). The AFCS design effort had paralleled and was completed during the phase 1 program. The AFCS consisted of maneuver camber control, maneuver load control, cruise camber control, and maneuver enhancement and gust alleviation (ME/GA). A description and discussion of the four modes is given in references 3, 4, and 5.

The foremost objectives of the phase 2 MFCS flight test program were to evaluate handling qualities, flying quantities, and A/C performance. In addition, the AFCS was evaluated by comparing results with the design predictions. Throughout both flight-test phases, there were no in-flight failures or system deficiencies that compromised safety or limited the flight-test objectives. A compilation of the AFTI/F-111 program and a summary of the flight-test results are given in reference 6.

ORIGINAL PAGE
BLACK AND WHITE PHOTOGRAPH

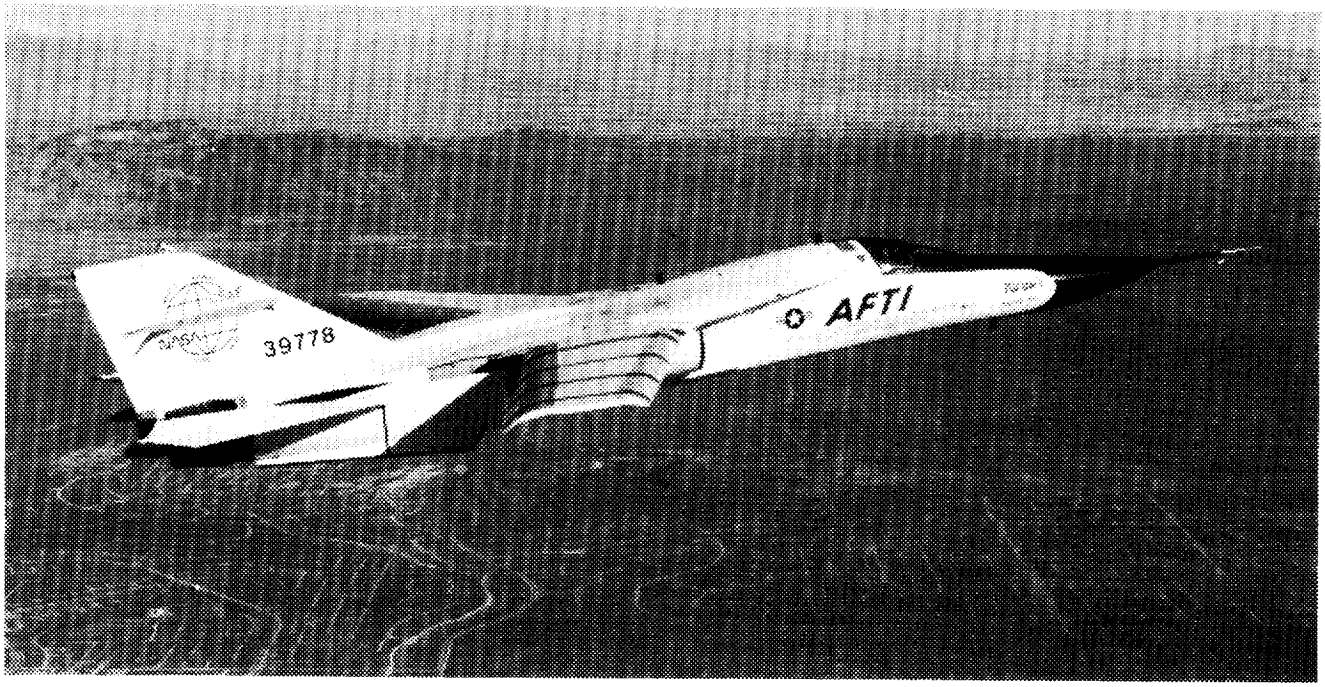

Figure 1. The AFTI/F-111 airplane.

This report discusses the AFTI/F-111 variable-camber control segments power actuating systems. A brief description of the A/C and wing modifications required to install the variable-camber wing is presented. Analytical descriptions of the MAW servoactuator feedback systems are given along with the predicted closed-loop frequency responses. The predictions are compared to measured frequency responses obtained during qualification and acceptance ground testing. Predictions, for example, are used to show the expected transient response during an exceptionally high dynamic pressure condition when coupled with a corresponding large hinge moment loading. The power demands of the hydraulic systems are assessed during an in-flight frequency sweep with the ME/GA mode engaged. In addition, the accumulated hours of MAW system operation are shown as a function of a chronology of the test events. The various types of failures experienced and the component and unit replacements required during both phases of the program are numerically tabulated as a function of the accumulated hours of operation.

The AFTI/F-111 MAW program was a combined effort by the NASA Dryden Flight Research Facility (DFRF), U.S. Air Force, Air Force Flight Test Center, Wright Research and Development Center, and Boeing Advanced Systems Company.

TESTBED AIRCRAFT

The following sections provide a general description of the basic F-111A aircraft, the AFTI/F-111 aircraft configurations, and the integrated primary control systems for both aircraft. The extensive modifications made to the TACT wing to implement the AFTI/F-111 variable-camber mechanical systems are highlighted in a limited review. Minor, but necessary, changes to the primary and utility hydraulic systems of the aircraft to obtain the necessary control rates and authorities are discussed and illustrated. Basic descriptions and information diagrams of the architecture are presented showing the signal flow from and to the MAW computers, primary and backup flaps, and flaperon servoactuator systems. The AFTI/F-111 pertinent physical and geometric characteristics are shown in table 1.

Table 1. The mission adaptive wing physical and geometric characteristics.

Wing (Λ = 16°):	
Area	623.2 ft^2
Aspect ratio	5.6
Taper ratio	0.636
Span	59.07 ft
MAC	10.9 ft
Leading edge of MAC	Fuselage station 471.276
Airfoil	Boeing Advanced Transonic Airfoil
Sweep range	16 to 58°
Thickness ratio:	
BL 93	9.7 percent
BL 321.9, tip	5.44 percent
Incidence:	
Jig, span station 124	−3.15°
Shape, span station 356	−6.70°
Dihedral	0°
Wing (Λ = 26°):	
Area	618.7 ft^2
Aspect ratio	4.95
Span	55.34 ft
MAC	12.67 ft
Wing, Λ = 58°:	
Area	605.8 ft^2
Aspect ratio	2.63
Span	39.93 ft
MAC	18.09 ft
Pivot location:	
FS 487.61	
BL 70.3	
Leading-edge flap:	
Type	Smooth variable camber
Number, on each side	1
Area, each flap	29.8 ft^2
$\bar{q}$ limit	1800 lb/ft^2
Flaperons:	
Type	Smooth variable camber
Number, each side	3
Area, each flap:	
Inboard	20.5 ft^2
Middle	20.9 ft^2
Outboard	17.1 ft^2
$\bar{q}$ limit	1800 lb/ft^2, maximum deflection up to 850 lb/ft^2

F-111A Basic Primary Control System

The F-111A testbed aircraft, an early version of the production F-111's, was fitted with a super-critical wing and was redesignated by NASA as the TACT/F-111 aircraft. The F-111A aircraft, a two-place, side-by-side fighter with two engines, could vary the wing sweep from 16 to 72°.

Pitch and roll control, in part, are accomplished by stabilons (fig. 2). Additional lateral control was originally provided by electrically commanded spoilers located spanwise and centered along the upper wing surface. Basic primary control in pitch and roll was derived by and through a triplex electronic rate command system with an overlapping direct mechanical system. In pitch, the stick commands a constant response proportional to the sum of pitch rate and normal acceleration ($\dot{\theta} + 4A_n$). The error signal is driven continuously to zero by a series trim actuator located in the forward loop (type 1 system). In roll, the lateral stick commands roll rate through both the rolling tail and the spoilers. The actual roll response thus depends on the error signal which is the commanded response minus the sensed roll rate feedback (type 0 system).

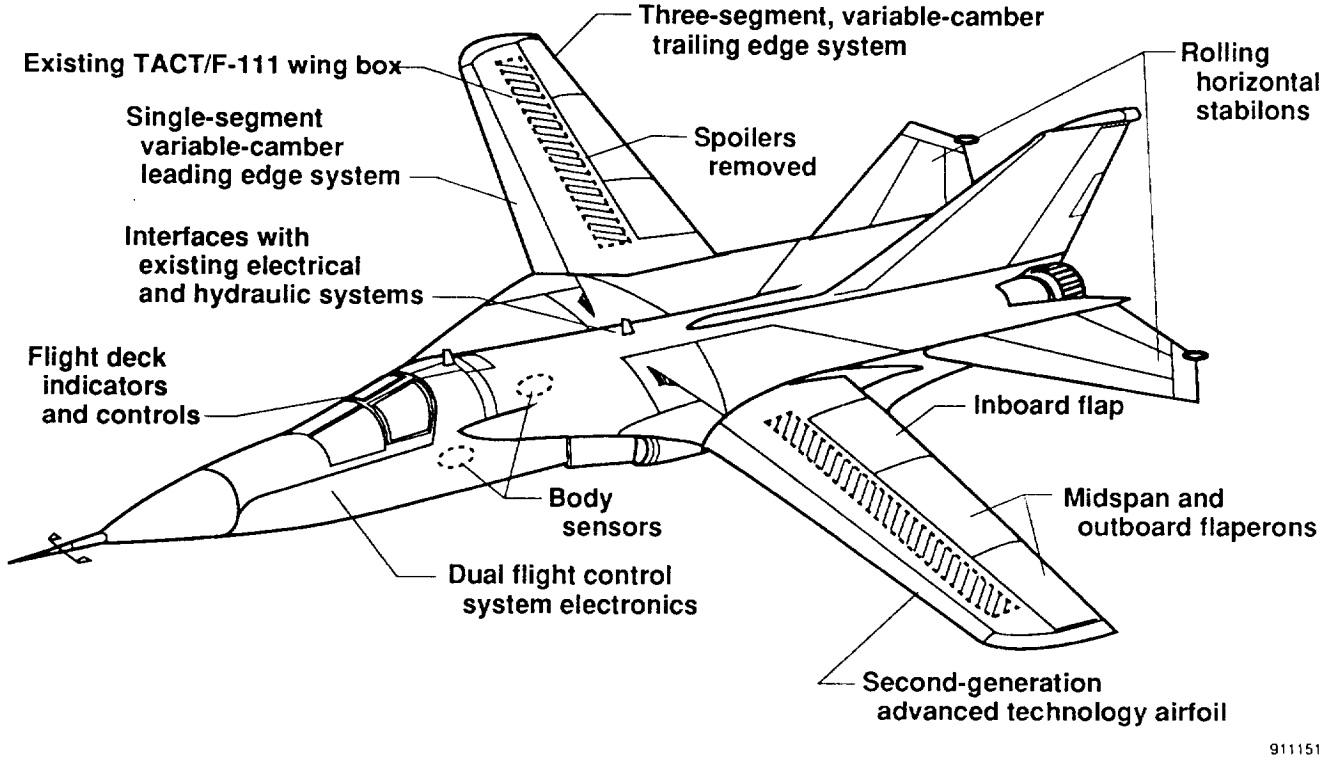

Figure 2. The AFTI/F-111 mission adaptive wing.

The feedback rate signal in both the pitch and roll axis provides the artificial damping. Adaptive gain changes are located in the forward loop of both the pitch and roll axis and are unique to all F-111 A/C. This F-111A A/C has the option of manual selectable gains. In the yaw axis, a simple fixed-gain, rate-damper system provides artificial yaw damping. Lateral acceleration and washed-out yaw rate sum as feedback and proportionally drive the rudder in a typical yaw-damper fashion. All three flight control axes are triplex redundant with middle value selection. A more comprehensive description of the F-111A control systems is given in reference 7.

AFTI/F-111 Hardware and Mechanical Systems

Modification and construction of the AFTI/F-111 MAW used the existing TACT wing box, the wing pivots, plus the fixed portions to the LE and TE, indicated as TACT in figure 3. The LE on each wing consisted of one continuous segment flexed through linkages and nine rotary actuators driven by two PDU's at each end of the segment. The TACT spoilers were removed and their roll control function replaced by four TE flap segments. Each of the three TE flap segments was controlled by individual systems. The three segments was necessary because of the higher aerodynamic hinge moment loading anticipated on the TE. Each outboard, midspan, and inboard TE segment was driven by two PDU's located at each end of the respective segment. The midspan and outboard flaps provide, in part, the lateral control and are called flaperons.

Rotary motion was transferred from the PDU's to the rotary actuators by a torque tube drive shaft. The PDU's and rotary actuators had a combined gear ratio of 975:1. In addition, the PDU's were mounted and grounded along a spanwise line near the wing box or on the added load-carrying structure. Each segment incorporated flexible fiberglass skins on the top panels and metal sliding panels on the bottom panels. The bottom panels were overlapped at the junction to provide a continuous and nearly uninterrupted surface. Flexing and controlling the camber of each segment involved deforming the upper panels of the LE and TE through a scissor and part-grounded linkage arrangement. The linkages also transferred the translational motion from the rotary motion of the actuators, as shown by typical flap sections (figs. 4(a) and (b)). A more complete description of the design, structure, and mechanical system is given in reference 8.

The electroservo-controlled hydraulic PDU had a hydraulic supply manifold, a hydraulic motor, a 0.727:1 input–output gearbox, and a motor control valve module. The electrical components of the motor control valve module are comprised of the servovalve, the pressure transducer, and the blocking and bypass solenoid valves (fig. 5). Electrical brakes were attached to the gearboxes on the TE PDU's and on the LE actuator shaft ends (fig. 3). Because of the larger actuating area for each PDU, larger motors, 0.62 in^3 in displacement (CID), were used on the LE. The motor size on the TE flaps and flaperons was 0.365 CID. The PDU's, electrical components, and rotary actuators had been flight qualified and used in some mechanical controlling functions on other aircraft. On the other hand, the complete integrated PDU package, actuators, and dual implementation were extensively ground tested by the contractor and NASA before and during the final ground test phases (ref. 9).

AFTI/F-111 Hydraulic Systems

Hydraulic power for the variable-camber wing PDU's is derived from and connected to the basic TACT/F-111 primary and utility hydraulic power supply systems (ref. 10). The two TACT/F-111 systems are completely and logically isolated from each other. Originally, two stock 42 gal/min pumps on each engine, one primary and one utility, supplied 3000^+ lb/in^2 hydraulic power in a parallel fashion to the two systems. With the spoilers eliminated, that portion of the hydraulic power allocation was available for the MAW systems. Addition of the 16 PDU's caused an increase in demand for hydraulic power which was considerably higher than the spoiler had previously required. Model studies determined that an increased hydraulic capacity was necessary. As a result, the stock F-111A hydraulic pumps were returned to the manufacturer and were upgraded from 42 to 47 gal/min, an 11-percent increase.

Similar modifications were required for the primary and utility systems to implement the variable-camber wing (fig. 6). Each cambered segment was driven by two PDU's located on the end of each segment (fig. 3). One PDU was powered by the primary system. The other PDU was powered by the utility system. If a system should fail, control of any segment would be available through a single PDU; however, such control would be limited to a lesser aerodynamic load condition, restricted surface authority, or reduced response. The LE flaps were driven by 11.3-gal/min PDU motors, and the TE flaps and flaperons were driven by 16.6-gal/min PDU motors. Four accumulators were

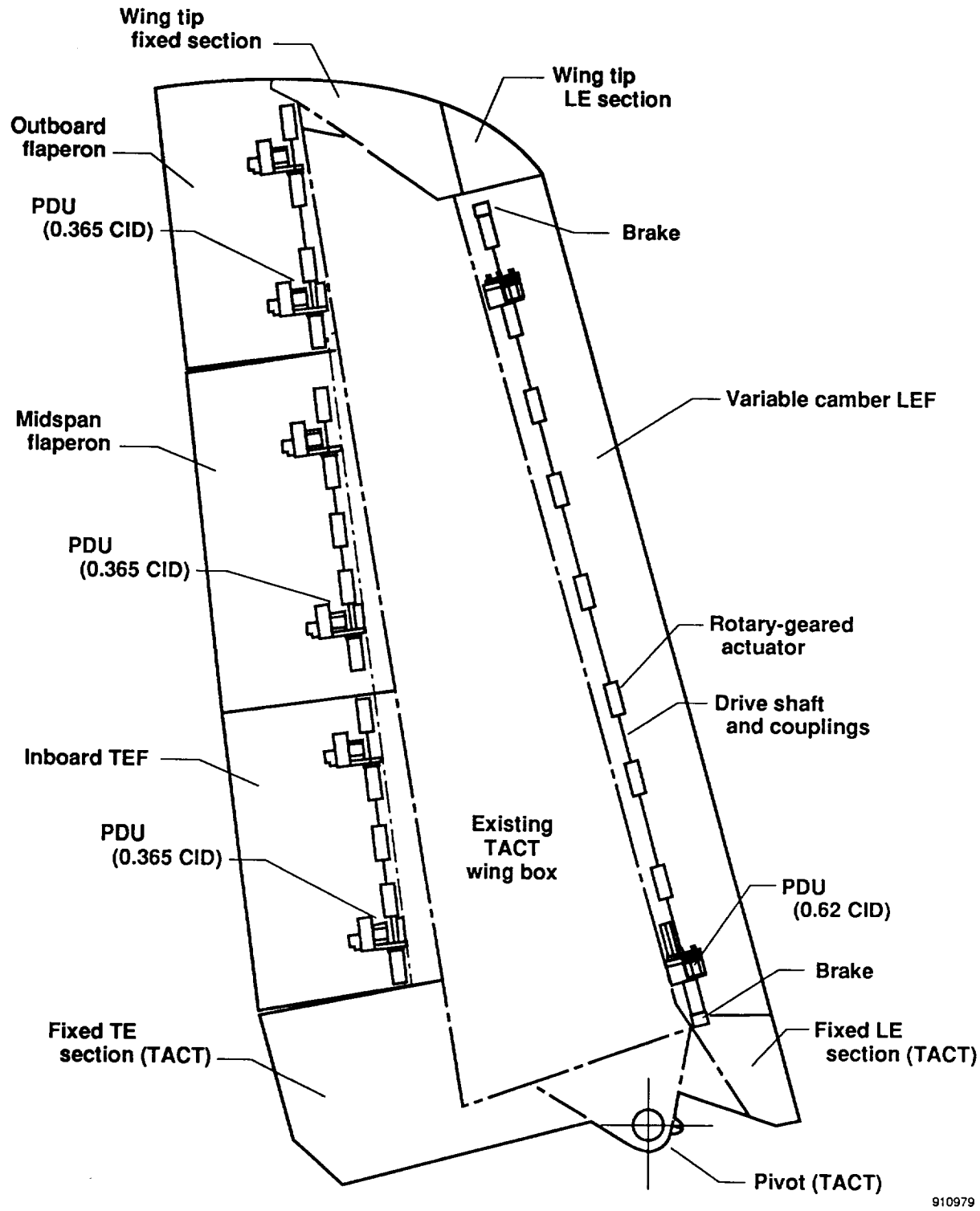

Figure 3. Mechanical systems used in flexing the leading and trailing edges of the variable-camber wing.

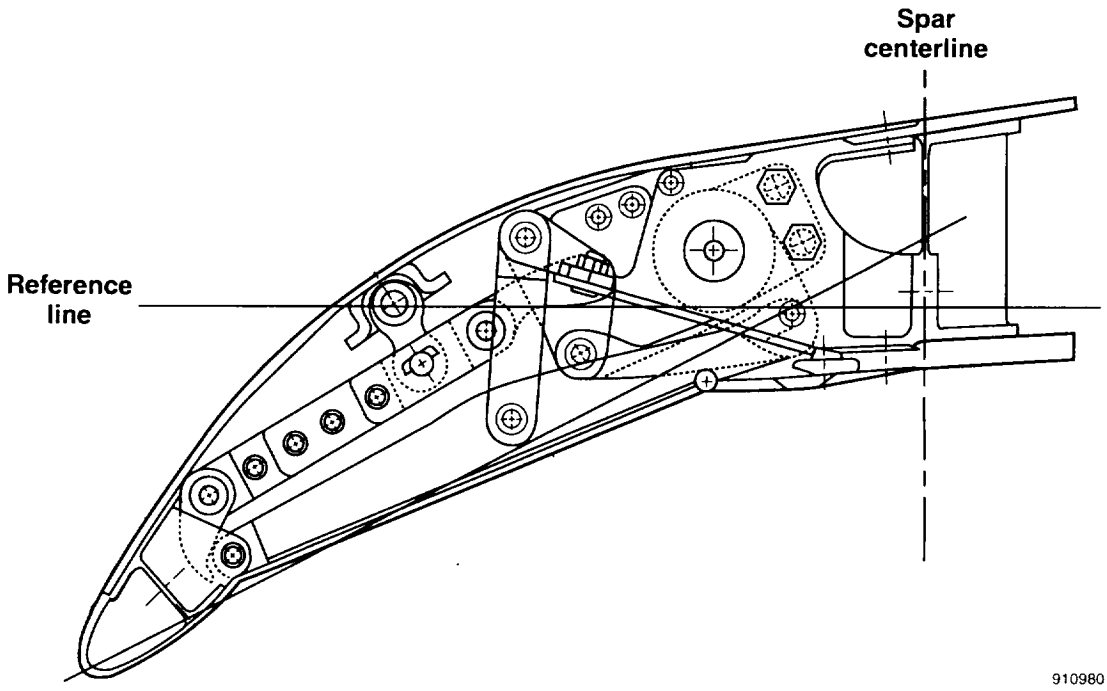

(a) Leading-edge section.

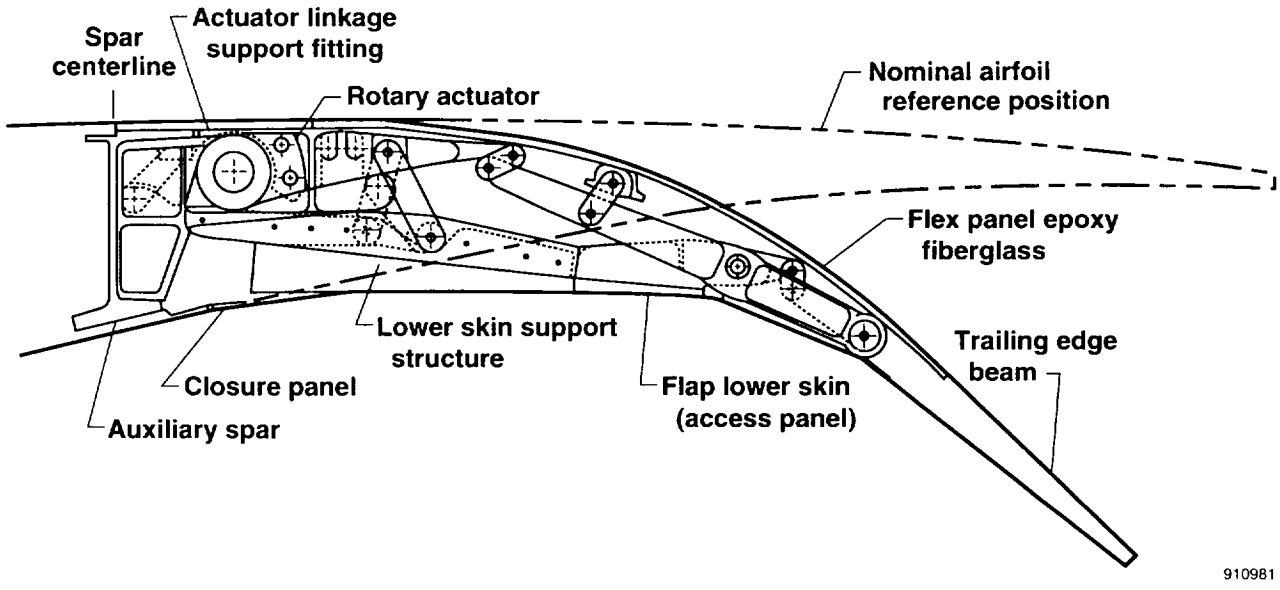

(b) Trailing-edge section.

Figure 4. Leading- and trailing- edge flap linkages in the fully deployed position.

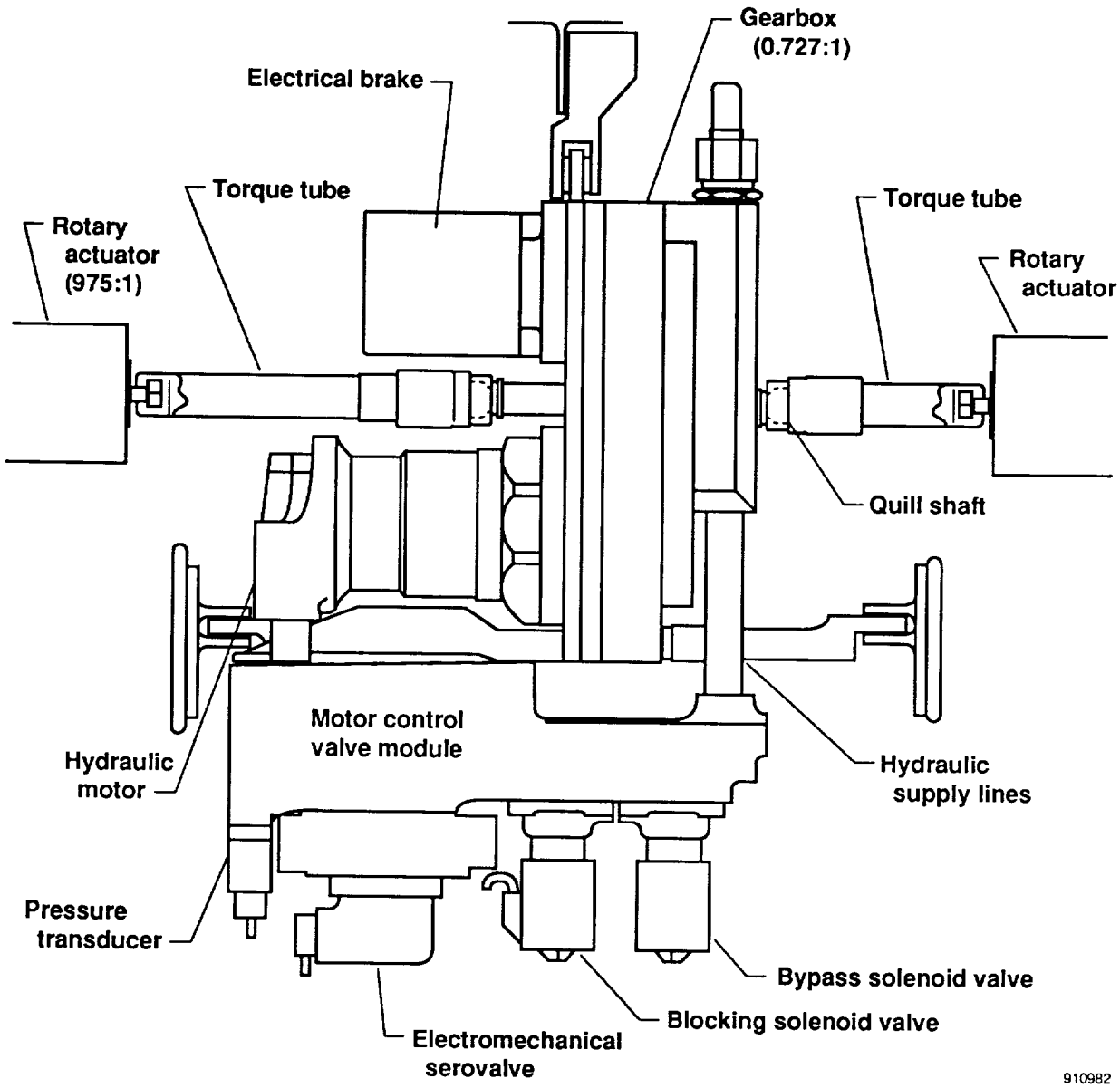

Figure 5. Power drive unit and electrical components.

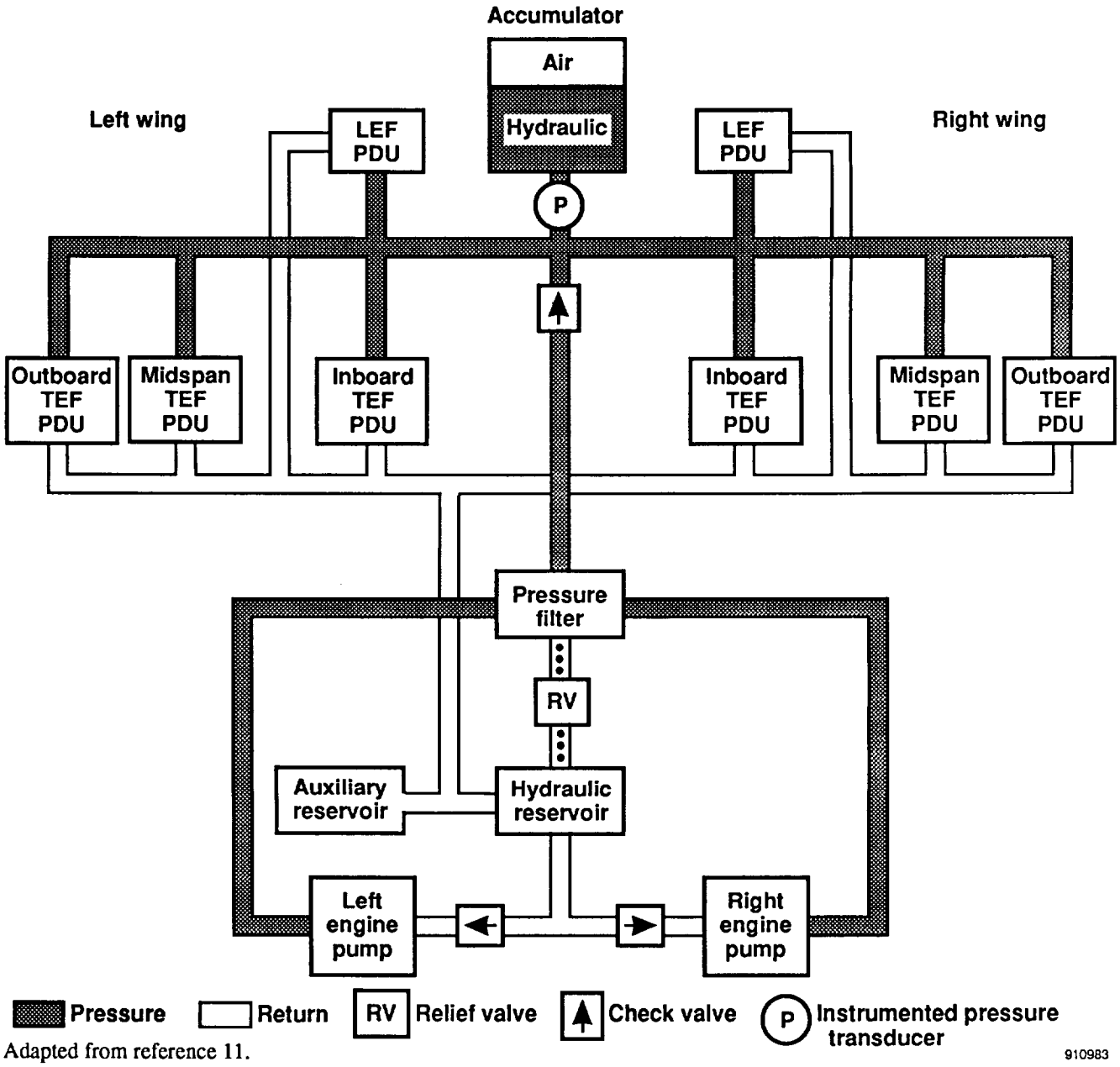

Adapted from reference 11.

Figure 6. Modified AFTI/F-111 mission adaptive wing primary and utility hydraulic systems.

added, two to each wing system. When precharged to 1100 lb/in^2, the accumulators provided an additional capacity of 0.87 gal/unit. A 1.3-gal auxiliary reservoir was added to the primary system to accommodate the increased capacity required by the added accumulators. Of necessity, the basic aircraft utility system had sufficient reservoir capacity. A more detailed description of the F-111A and MAW hydraulic systems and requirements is provided in references 10 and 11.

Manual Flight Control Systems

The MAW flight control systems were designed and implemented to functionally provide for both primary and backup control. The digital software, control logic, and electronics of both systems reside in the flight control electronic units (FCEU's). The software and fly-by-wire systems are dual-redundant. The MAW system independently adds roll command with the roll rate command augmentation system (CAS) of the basic aircraft.

The MAW primary systems use digital computers programmed with gains, algorithms, and logic to provide inputs to the servoelectronics which, in turn, drive the PDU's. The MAW backup systems are completely analog and provide the fail-operational reversion system for controlling TE flaperons and for positioning the inboard flaps. Backup control is activated automatically as a downmode decision of the failure and fault detection logic; however, the backup systems can be manually selected by the crew. In an emergency, both primary and backup MAW systems could be disengaged and the aircraft flown with the basic CAS. With CAS only, roll control power is derived from differential stabilon deflection. Although this configuration is limited, sufficient roll control power is available to fly and land the airplane.

Primary and Backup Systems Architecture

The digital and analog systems architecture, in part, is shown in figures 7(a) and (b). The 16 PDU's are designated by numbers in the upper corners of the control segments. Surface commands to both systems are directed to and through the FCEU's. The primary system (fig. 7(a)) is partitioned so that each PDU on each control segment normally receives an identical command from its respective channel. In addition, the position feedback by the primary system linear voltage differential transformers (LVDT's) are independent of each other. The measured position is fed back to the respective channel.

With the MAW backup system engaged (fig. 7(b)), the PDU's of the midboard and outboard TE segment receive analog commands from the same channel. The PDU's are grouped as follows: channel A controls the left midboard and right outboard, and channel B controls the right midboard and left outboard. The cambered position of each segment is determined by only one LVDT; therefore, a common signal is fed back to both channels. The PDU's on the inboard segments are positioned individually, but symmetrical inputs or commands from each channel drive them together. In the backup mode, the LE flaps are disengaged and braked at the existing positions. The flaps remain in the braked position. A more complete description of the MAW systems, redundancy management, and reversion logic is given in reference 2.

Servoactuator Control Systems

A block diagram of the basic servoactuator control loop is shown in figure 8. In the primary mode, the digital position command is converted to an analog signal. Then, the error signal ε proportionally directs the electromechanical flow control valve in the PDU. The PDU motor acts as an integrator, integrating the flow rate and translating the surface by the number of motor revolutions. The actual position of the surface is measured by the LVDT position signal and demodulated by the feedback electronics. The sum of the position command reference signal and the feedback signal, scaled 0.77 V direct current (Vdc)/deg, gives the error signal. Because of the integrator (type 1

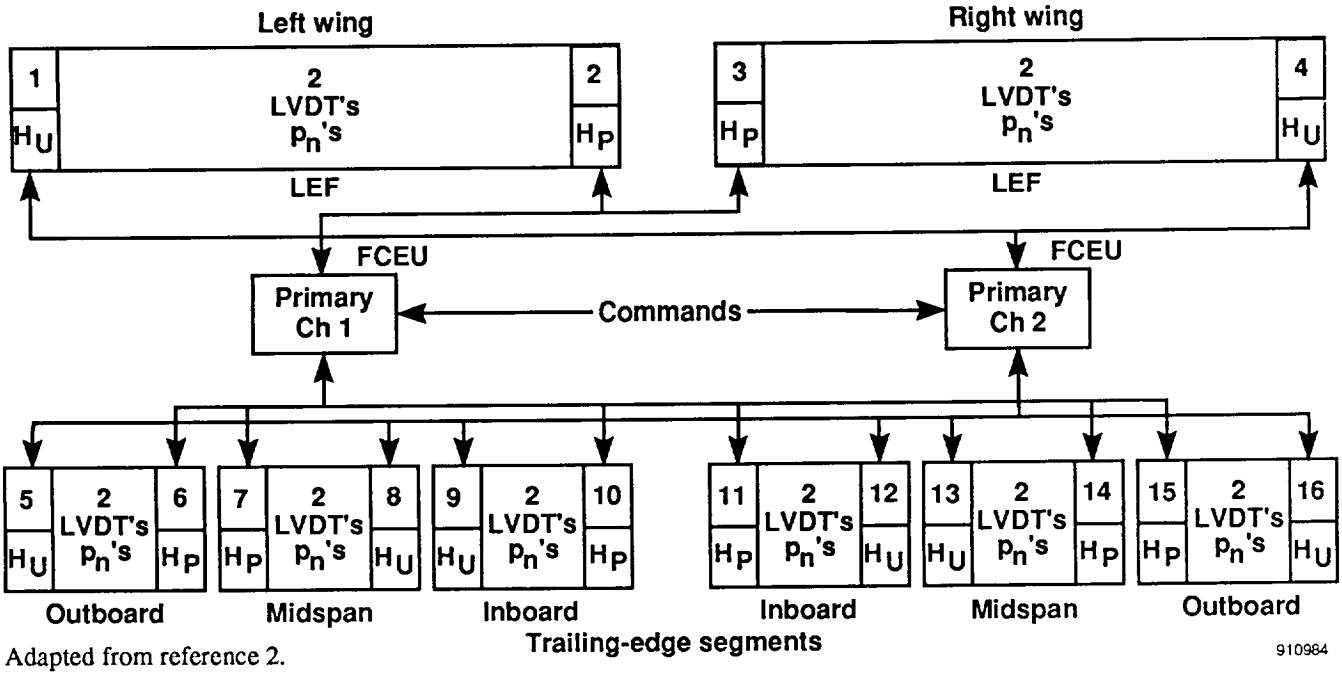

Adapted from reference 2.

(a) Digital primary systems.

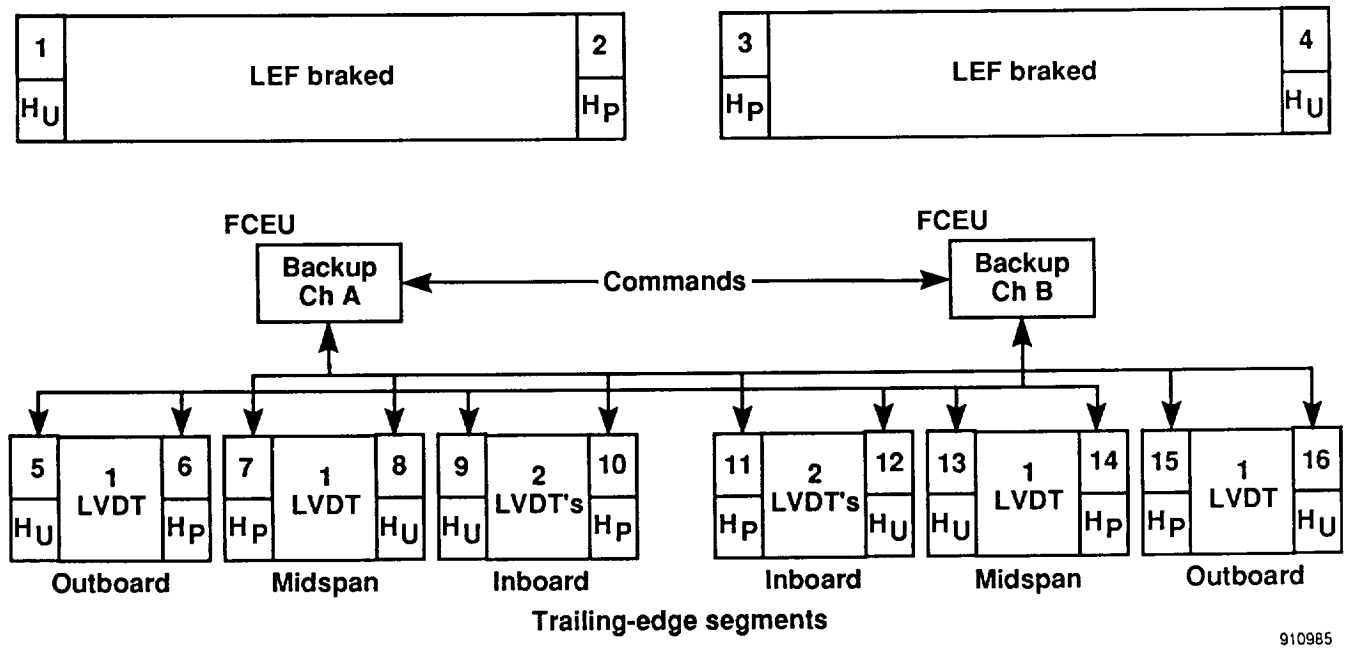

(b) Analog backup systems.

Figure 7. The mission adaptive wing flight control system architecture.

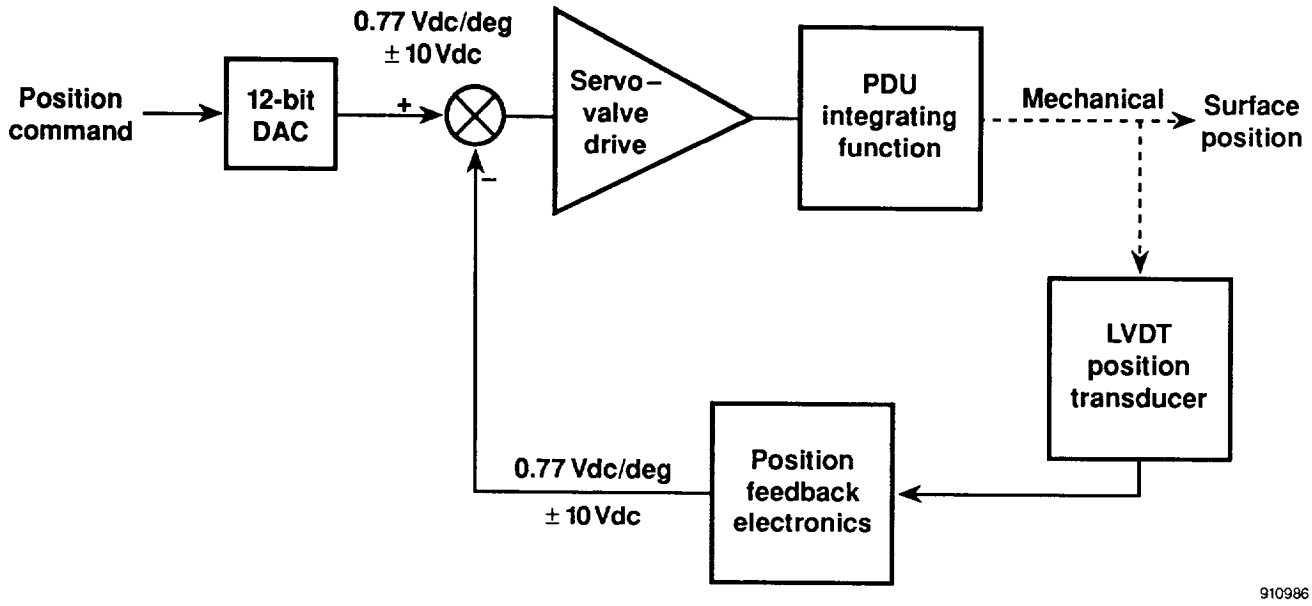

Figure 8. The basic servocontrol loop.

system), the error signal is continuously driven to zero; therefore, the actual surface position follows the desired position commands. The backup servocontrol loops are the same, except for the position command which is scaled and ranged directly as Vdc feedback.

In the primary mode, identical dual-channel systems position and control the variable-camber segments. Figure 9 is a block diagram of a typical flap showing the complete dual-channel structure of the servoactuator control systems. This figure also shows the equalization and paired variable-camber control. Except for slight gain changes, this example is common for all eight variable-camber control segments. The complete system characteristics, including uncommon gains, are given in table 2 for each control segment. The two channels shown by the FCEU's and servoelectronics employ error and delta pressure equalization loops to minimize the force-fight that may develop from separate PDU mechanical inputs to a common torque shaft. Almost identical commands from the FCEU's are summed, respectively, with the individual LVDT feedback signals. The two error signals are compared. Next, one-half of the difference is added and subtracted to the actuating signal of each channel. Thus, error equalization loops give identical actuating signals regardless of the feedback.

Pressure equalization minimizes, in part, the force-fight caused by the offset difference in the driver amplifiers and servovalves. Pressure sensors detect the delta pressure across the valve that, when compared, is indicative of the pressure reaction caused by the opposing torques. Electrical difference is used for feedback and summed with the actuating signal. The assigned gain on the compared signal was experimentally determined using a full-scale mockup.

The maximum rates and control surface authorities are listed in table 3. The midspan and outboard flaperons that supplement the roll power produced by the rolling tail were designed to respond at 40 deg/sec. The maximum upward travel of all surfaces is limited to approximately $-1°$, and the maximum downward travel is approximately 20°. More complete descriptions for the position and pressure equalization and failure limitations are in reference 12.

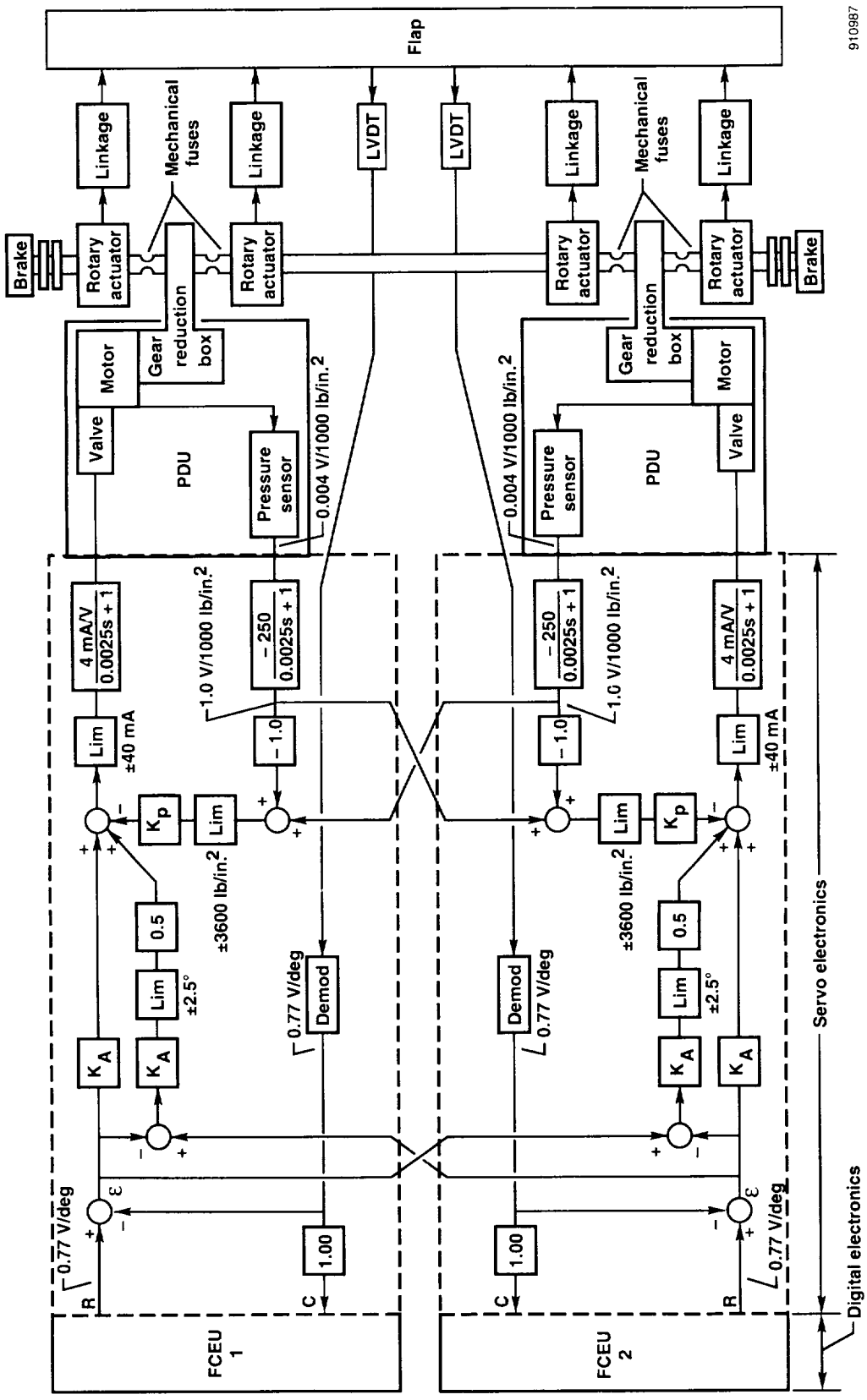

Figure 9. The servoactuator system.

Table 2. Hydraulic servoactuator characteristics and analytical constants, reference gain and LVDT gain = 0.77 V/deg and range ±10 V.

Element and Function	Units	Leading Edge	Inboard	Midspan	Outboard
System gain, $K_e = (K_A \times 57.3 \times 0.77)$	$\frac{V}{rad}$	$K_A = 3.04$ $K_e = 134.13$	$K_A = 1.92$ $K_e = 84.71$	$K_A = 1.08$ $K_e = 47.65$	$K_A = 1.08$ $K_e = 47.65$
Pressure equalization gain: K_P	---	$K_P = 0.124$	$K_P = 0.110$	$K_P = 0.09$	$K_P = 0.09$
Valve drive amplifier, first order: K_D, τ_D	$\frac{mA}{V}$	$K_D = 4.0, \tau_D = 0.0025$			
Servovalve, first order: K_{sv}, τ_{sv}	$\frac{in.}{mA}$	$K_{sv} = 0.0023, \tau_{sv} = 0.0227$			
Servovalve flow gain, K_Q	$\frac{in^4}{\sqrt{lb \cdot in \cdot sec}}$	$K_Q = 66.167$			
Pressure gain, $\sqrt{P_s \pm P_\Gamma}$	$\frac{\sqrt{lb}}{in.}$	$P_s = 2925$, P_Γ variable			
Motor displacement, gain: $\frac{1}{D_m}$	$\frac{rad}{in^3}$	$\frac{1}{0.09868}$	$\frac{1}{0.05809}$	$\frac{1}{0.05809}$	$\frac{1}{0.05809}$
Integrator, $\frac{1}{s}$	$\frac{sec}{rad}$	---	---	---	---
Gear ratio, motor to actuator: $\frac{1}{n_t}$	---	$\frac{1}{708.7}$			
Gear ratio, actuator to surface: $\frac{1}{n_t}$	---	$\frac{1}{3.43}$	$\frac{1}{2.819}$	$\frac{1}{1.969}$	$\frac{1}{1.969}$
Feedback filter, first order: K_{F1}	---	$\frac{1}{0.0032s+1}$			
Feedback filter, second order: K_{F2}	---	$\frac{314^2}{s^2+2\times0.5\times314s+314^2}$			

Table 3. Control surface rates and authorities of the variable-camber wing.

Control surface	Rate, deg/sec	Position limits, deg Up	Down
Leading edge	10	−1.07	20.63
Trailing edge:			
Inboard flaps	30	−1.08	17.87
Midspan flaperon	40	−0.69	19.74
Outboard flaperon	40	−0.71	19.59

Source: Reference 2.

HINGE MOMENT ANALYSIS

The variable-camber TE is usually positioned near zero or in a downward direction. The flaperons are differentially flexed from that position. When the control segments are down, there is always some constant hinge moment torque on the mechanical system caused by flexing the upper surface. In flight, when aerodynamic forces are present, the TE hinge moment torques are generally much larger than torques on the ground. These two torque moments are additive and totally opposing to any further downward travel of the flaperons. On the LE, however, the corresponding hinge moment torques are normally less than those torques experienced on the TE. These corresponding torques may sum up as alleviating forces, depending on the amount of twist and the local angle of attack. In subsequent sections, these hinge moment torques are treated as feedback functions that change the pressure gain according to the magnitude of the torque and whether the control flap is moving up or down.

Analytical Modeling and Definition

During the preliminary design phases, it was necessary to know the predicted hinge moment torques reflected as force feedback through the mechanical system back to the PDU motors. Wind tunnel tests were conducted to obtain the aerodynamic hinge moment coefficients of the surfaces at various cambered positions. Then, these data along with desired rates were used to size the hydraulic systems, complete the final design, and provide the schedules for limiting the surface authority as a function of impact pressure. Figure 10 shows an analytical model of the servoactuator control system. System parameters and constants used in subsequent calculations are listed in table 2. Generally, the gains, time constants, and gearing ratios in table 2 were used during the simulation and were taken from reference 13.

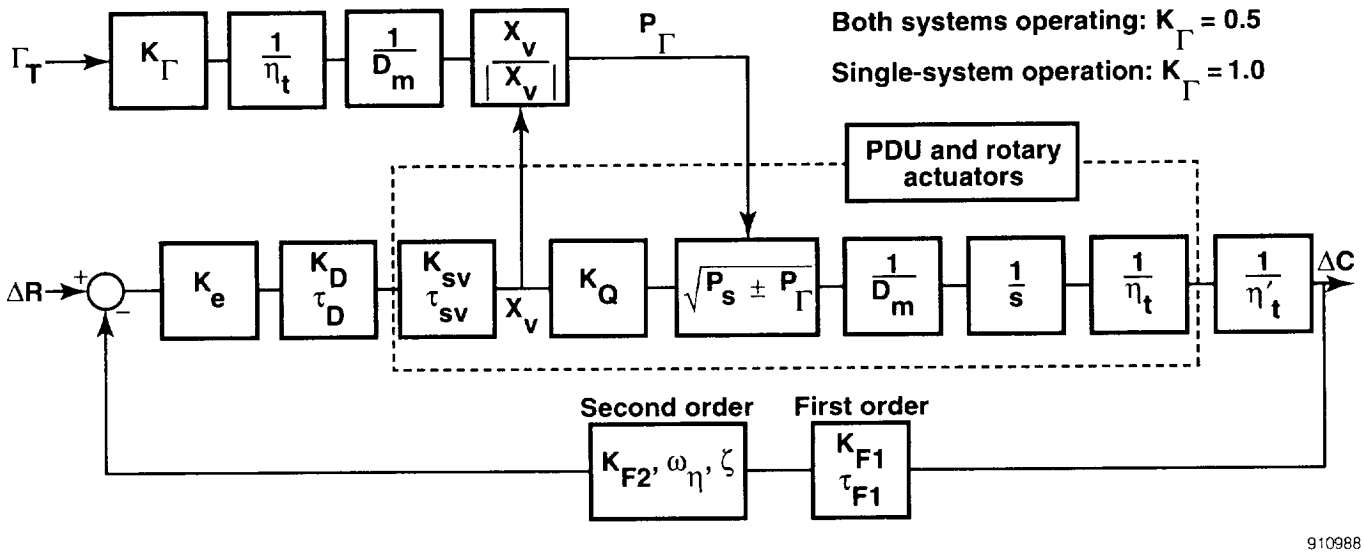

Figure 10. Equivalent model of the hydraulic servoactuator.

Describing and predicting the exact characteristics of the servoactuator presents some difficulties because of the nonlinearity of the pressure gain term $\sqrt{P_s \pm P_\Gamma}$ (fig. 10). As shown, this term depends on the external torque and governs the rate of flow. Basically, the rate of flow Q in a hydraulic servoactuating system is proportional to the square root of the pressure drop ($Q \propto \sqrt{\Delta P}$). For systems where external load forces F_Γ are present, the net vector force across the face of each piston or displacement element is shown in the simplified force diagram (fig. 11) where

P_R = return pressure, approaching zero,

P_s = operating or supply pressure drop,

F_Γ = generalized total force, aerodynamic plus the flexing load, and

F_N = net resultant force caused by P_s and P_Γ.

Because of the high gear ratio, the external load F_Γ is considered constant for each displacement element in the PDU motor as

$$F_\Gamma = P_\Gamma \times A \tag{1}$$

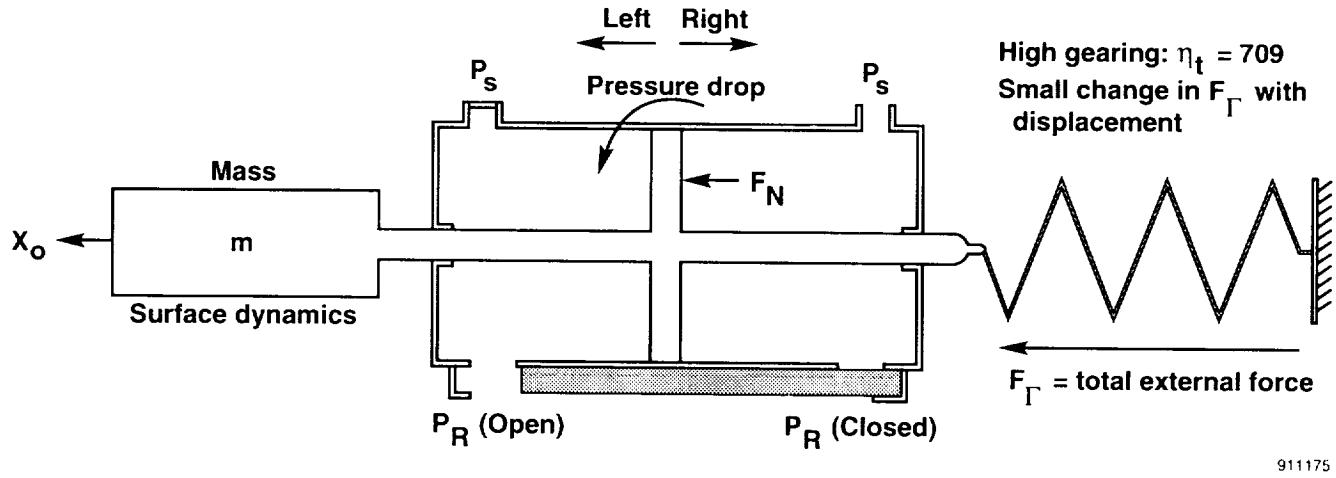

Figure 11. Simplified force diagram of a power drive unit displacement element.

Thus, P_Γ is thought of as a mechanical pressure, the result of the external load, so that movement to the left would cause a net force equal to

$$\overleftarrow{F_N} = \overleftarrow{P_s} \times A + \overleftarrow{P_\Gamma} \times A = (P_s + P_\Gamma)\, A \text{ (up flap)} \tag{2}$$

The net force in movement to the right would be

$$\overrightarrow{F_N} = \overrightarrow{P_s} \times A + \overleftarrow{P_\Gamma} \times A = (P_s - P_\Gamma)\, A \text{ (down flap)} \tag{3}$$

Because the return pressure approaches zero, the total pressure drop is the algebraic sum

$$P_s \pm P_\Gamma \tag{4}$$

This value depends on valve position; therefore, the rate of flow integrated by the PDU motor is expressed in the common fashion as

$$Q = \overleftarrow{X_V}\ K_Q \sqrt{P_s \pm P_\Gamma} \tag{5}$$

where

X_V = servovalve position,

K_Q = servovalve flow gain, and

$\sqrt{P_s \pm P_\Gamma}$ = pressure force gain.

From equation (5), Q depends on the product of the valve position $\overleftarrow{X_V}$ and the magnitude of $\sqrt{P_s \pm P_\Gamma}$. The sign for the external force P_Γ is maintained analytically by the external loop (fig. 10).

In figure 10, the input ΔR is considered a small change about a trimmed condition. The control variable ΔC is the resulting change in surface position about the trimmed condition. During a frequency sweep, the total torque Γ_T causes either a back or an aiding pressure at all frequencies. This pressure alternately changes once over each control cycle; thus, the force gain $\sqrt{P_s \pm P_\Gamma}$ depends on the external torque Γ_T and supply pressure P_s plus the sign of the control value X_V. The force gain is, therefore, related to the closed-loop phase. It follows, then, that the pressure

gain is related to the dynamic characteristics of the system. Because the pressure gain is not constant, the extent of any linear analysis may be somewhat limited. Consider a condition with no aerodynamic loading, like on the ground, and with the outboard segment flexed all the way down. The total measured flexing torque is approximately 10×10^3 in·lb. With both PDU's operating, $K_\Gamma = 0.5$. The resulting change in hydraulic pressure would be

$$\Gamma_T \times K_\Gamma \times \frac{1}{\eta_t} \times \frac{1}{D_m} = 121.45 \text{ lb/in}^2 \tag{6}$$

For a 3000-lb/in^2 system operating at a typical supply pressure of 2925 lb/in^2, the expected variation in pressure gain is

$$52.9 \text{ (down flap)} \leq \sqrt{P_s \pm P_\Gamma} \leq 55.2 \text{ (up flap)} \tag{7}$$

As indicated, the variation in pressure gain caused by flexing is small. Consequently, the variation in frequency and transient response characteristics of the servoactuator would also be small. At high aerodynamic load conditions, however, this variation can be large, as shown later, and would require schedules to limit the authority of the flaps and flaperons.

Frequency Response

Frequency response tests were conducted by DFRF as part of qualification and acceptance testing. The tests were performed on the ground; consequently, the servoactuating system would only be experiencing the flexing and inertia loading. All surfaces were initially trimmed halfway down, approximately 11°. Random noise test methods were used with a signal analyzer, at a noise source level of 2° peak-to-peak, and over a frequency range of 0.5 to 25 Hz.

The measured and predicted frequency responses obtained for the LE, inboard, midspan, and outboard segments are shown in figures 12(a), (b), (c), and (d). The solid and dashed lines are the comparison between the right and left sides, respectively. The agreement between the right and left sides is consistent over the frequency range for all the segments. In particular, the flaperons, which constitute the primary control, show good agreement throughout. No lightly damped modes were detected over the frequency range investigated. Hysteresis was measured at the LVDT's during separate tests. When converted to surface travel, the threshold band was approximately ±0.06°. With a 2° peak-to-peak input, the perceptible level was above −24.5 dB, as indicated in the figures.

Analytical linear predictions were made using the values given in table 2. The results are indicated in figures 12(a) to (d). In general, the amplitude ratios are matched by the predictions. The phase, however, indicates more lag from the tests at the higher frequencies than the analytical model or transfer functions predict. The transfer functions derived from the closed-loop model are also presented in the figures. A second-order approximation can be obtained simply by canceling the higher order roots. This approximation typifies a control system having a natural frequency of approximately 30 rad/sec and a damping ratio between 0.51 and 0.62.

Predicted Transient Response Influenced by Torque Load

An example flight condition was selected near the maximum aerodynamic hinge moment torque loads, impact pressure q_c = 1000 lb/ft^2, to show the effect of torque on the servoactuator transient response. Figure 13 shows a MAW schedule that limits flaperon travel as a function of q_c. For the example calculation, the maximum flaperon travel is limited to approximately 15°. The wind tunnel hinge moment coefficient data in reference 13 were used to determine the torque loads. The maximum coefficient values occurred near Mach 0.9. Figure 14 shows the dynamic pressure as a function of Mach number at a constant q_c = 1000 lb/ft^2 and the q_c bounds for flaperon authority at $830 \leq q_c \leq 1360$. The dynamic pressure $\bar{q}$ is approximately 820 lb/ft^2. Hinge moment torques were determined

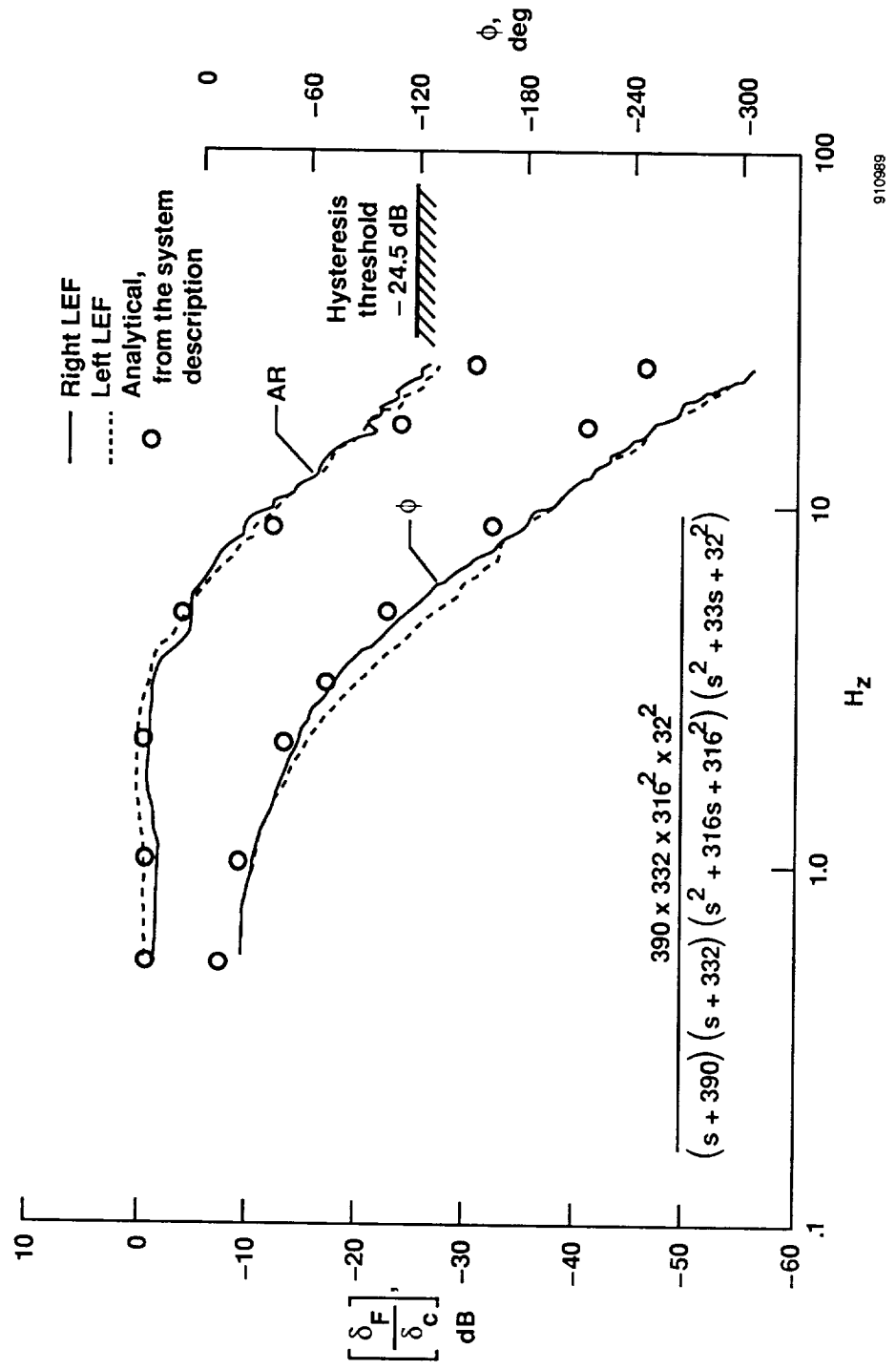

(a) Leading-edge flap.

Figure 12. Frequency responses of the variable-camber servoactuators during ground tests.

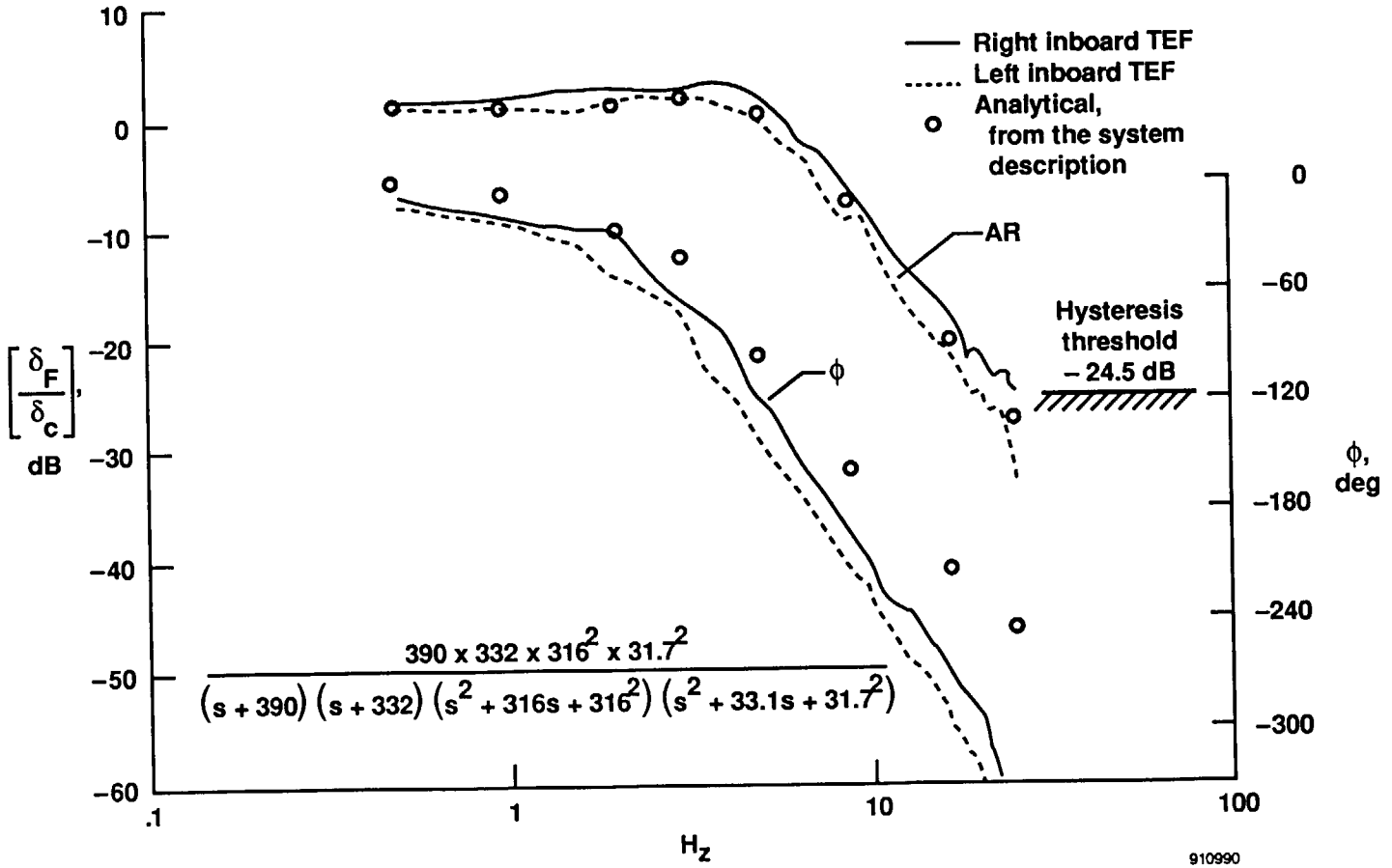

(b) Inboard trailing-edge flap.

Figure 12. Continued.

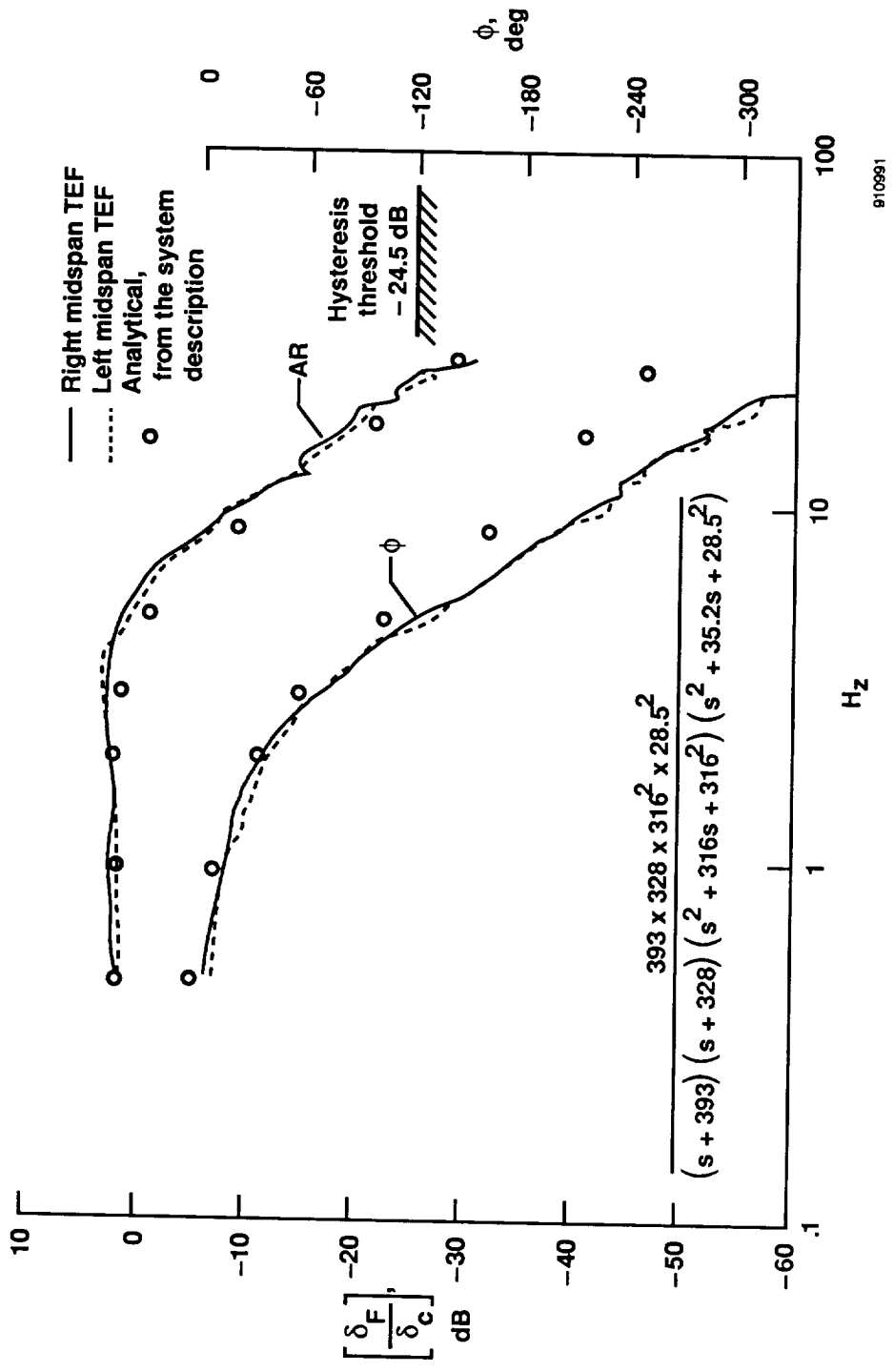

(c) Midspan flaperon.

Figure 12. Continued.

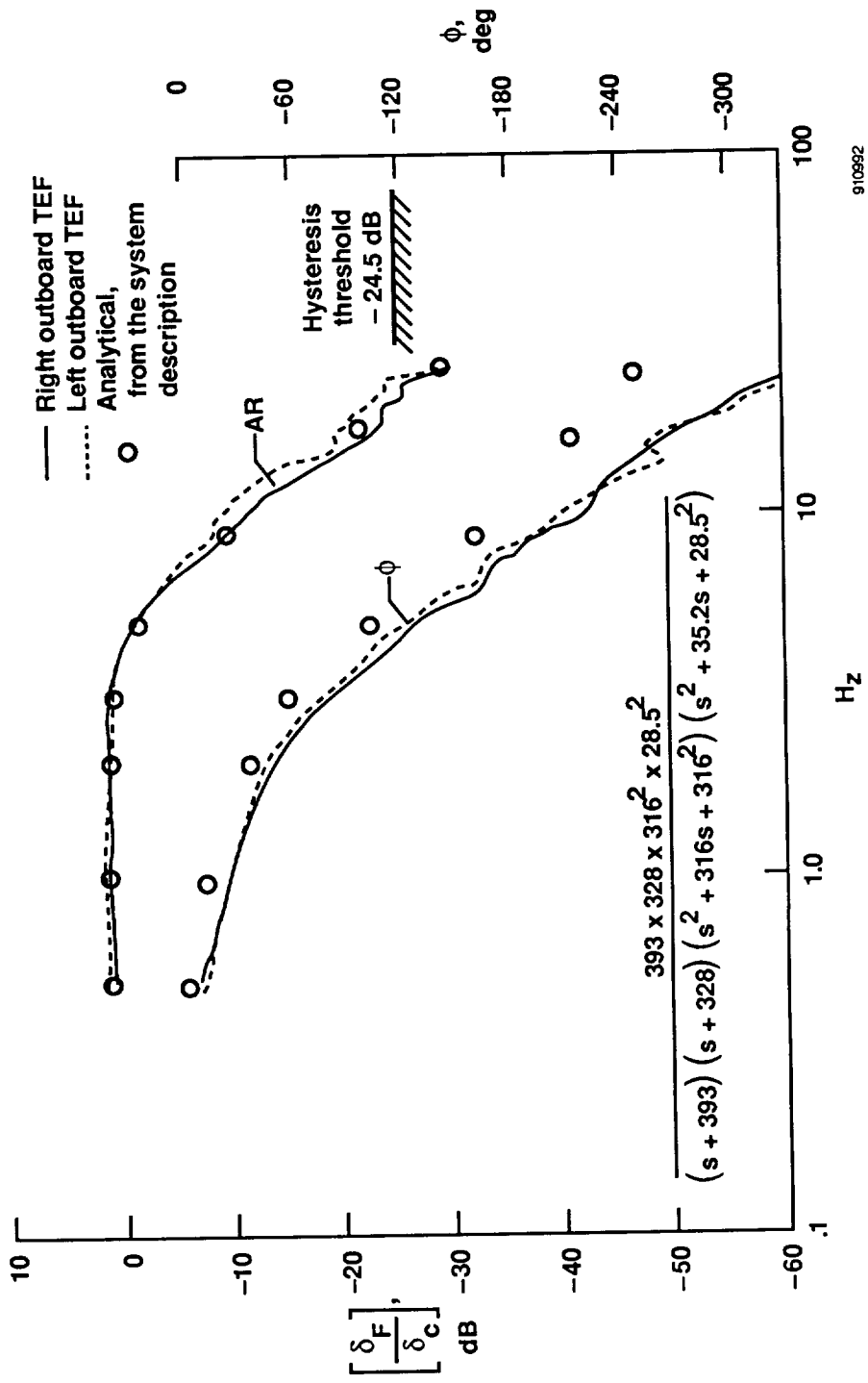

(d) Outboard flaperon.

Figure 12. Concluded.

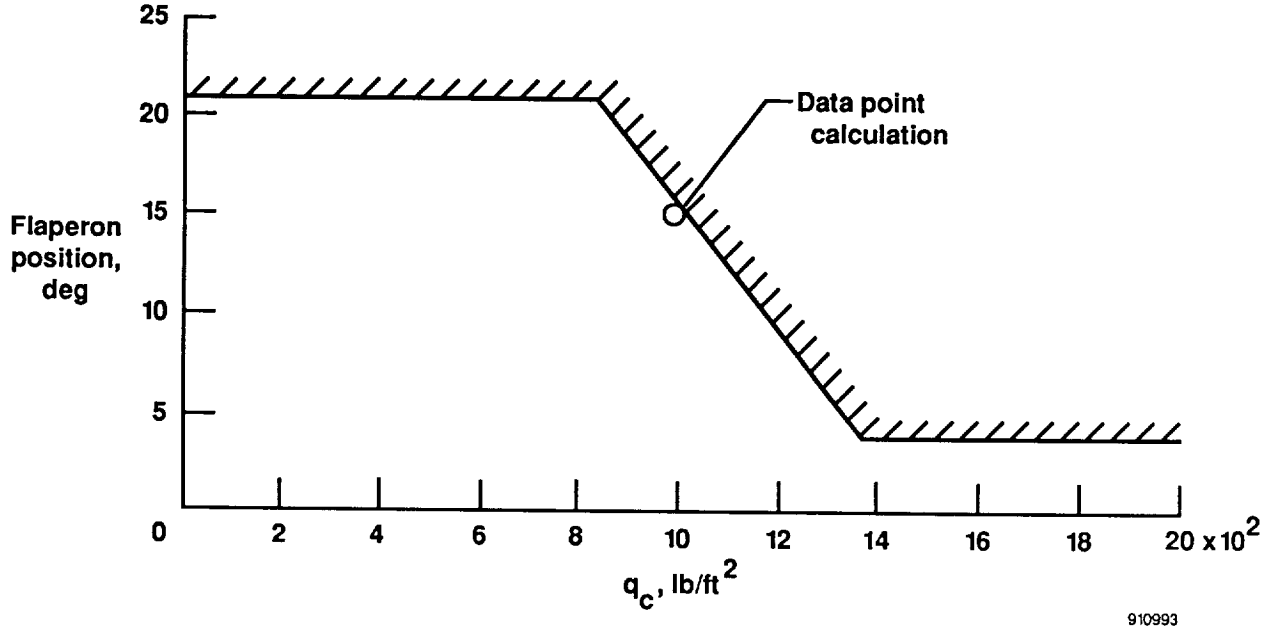

Figure 13. Flaperon position limit as a function of impact pressure, q_c.

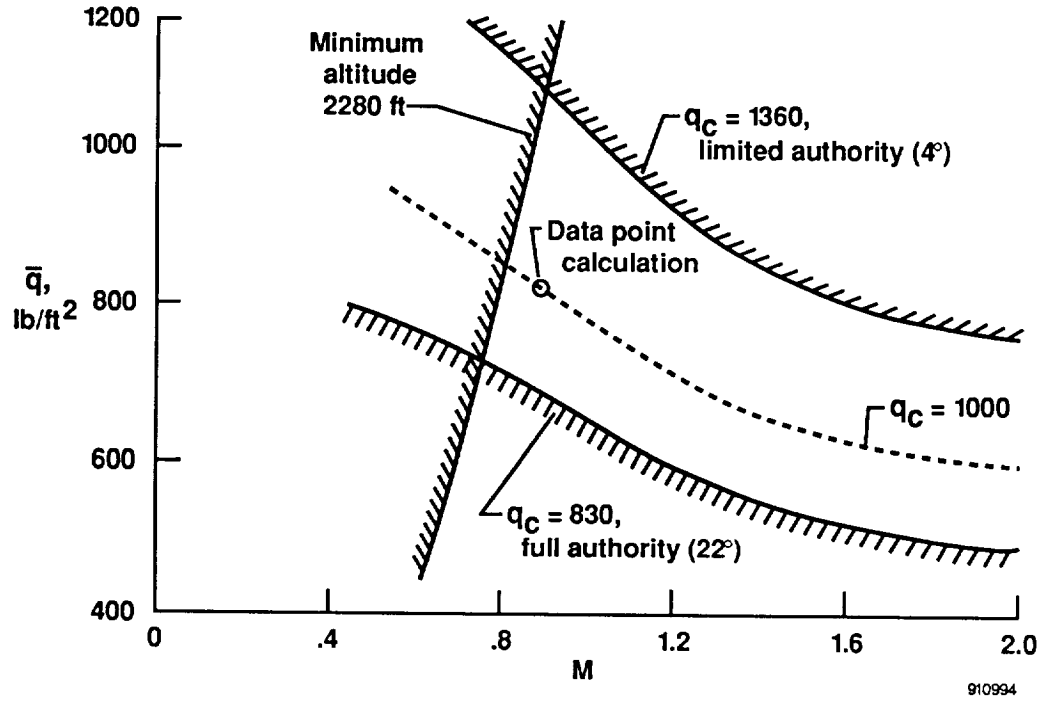

Figure 14. Variation of dynamic pressure with Mach number and impact pressure.

from the coefficients and dynamic pressure and are given in figure 15. The Γ_A was determined from wind tunnel data at $M = 0.9$, $\bar{q} = 820$ lb/ft^2, LEF = 0.0, and $\Lambda = 26°$ (ref. 13). Flexing torque Γ_F and hinge moment torque as a result of aerodynamics Γ_A are shown as a function of the outboard flaperon position. The equations for each curve are also given. Total torque for the example prediction at 15° deflection is

$$\Gamma_F + \Gamma_A = -90 \times 10^3 \text{ in·lb} \tag{8}$$

The pressure change is determined for an outboard flaperon servoactuator trimmed at 15° by using the maximum estimated torque. From figure 10 and table 2 with both PDU's operating at $K_\Gamma = 0.5$,

$$P_\Gamma = \Gamma_T \times K_\Gamma \times \frac{1}{\eta_t} \times \frac{1}{D_m} \times \frac{X_V}{|X_V|} = \pm 1093 \text{ lb/in}^2 \tag{9}$$

For a single PDU operating at $K_\Gamma = 1.0$,

$$P_\Gamma = 2186 \text{ lb/in}^2 \tag{10}$$

Thus, for a 3000-lb/in^2 system operating at a supply pressure of $P_s = 2925$ lb/in^2, the predicted pressure gain variation with both systems operating is

$$42 \text{ (down flap)} \leq \sqrt{P_s \pm P_\Gamma} \leq 63 \text{ (up flap)} \tag{11}$$

For single-system operation,

$$27 \text{ (down flap)} \leq \sqrt{P_s \pm P_\Gamma} \leq 72 \text{ (up flap)} \tag{12}$$

For no torque loads,

$$\sqrt{P_s} = 54 \tag{13}$$

The predicted linear transient responses of the example servoactuator systems operating at three different gains are shown in figures 16(a) and (b). The calculations were based on the following nonvariant conditions:

$$\begin{aligned} \text{TEF} &= 15° \\ M &= 0.9 \\ q_c &= 1000 \text{ lb/ft}^2 \\ \Gamma_T &= -90 \times 10^3 \text{ in·lb} \\ P_s &= 2925 \text{ lb/in}^2 \\ K_\Gamma &= 0.5 \text{ both PDU's} \\ K_\Gamma &= 1.0 \text{ single PDU} \end{aligned}$$

The rate limit boundaries are based on a ±5° step input. With both PDU's operating (fig. 16(a)), all curves exhibit responses with slight overshoots typical of linear second-order systems with damping ratios between 0.5 and 1.0. For a 5° step input with no hinge moment ($\sqrt{P_s} = 54$), the transient responses of the basic servoactuating system would be rate-constrained when the output exceeded 40 percent of the input. The upward response, with an alleviating hinge moment ($\sqrt{P_s + P_\Gamma} = 63$), would be rate-constrained starting when the output exceeded 30 percent of the input. The downward step input, against an opposing hinge moment $\sqrt{P_s - P_\Gamma} = 42$, reduces the transient response to a full linear system. Figure 16(b) shows the responses with one PDU operating. It is like doubling the hinge moment function to the same servomechanism of $K_\Gamma = 1.0$. Comparisons are made to the basic system with no hinge moment function that has a damping ratio of $\zeta = 0.62$. When the servoactuator is aided by the pressure gain $\sqrt{P_s + P_\Gamma} = 72$ following an upward step input, the damping ratio is reduced to $\zeta = 0.5$. A downward step

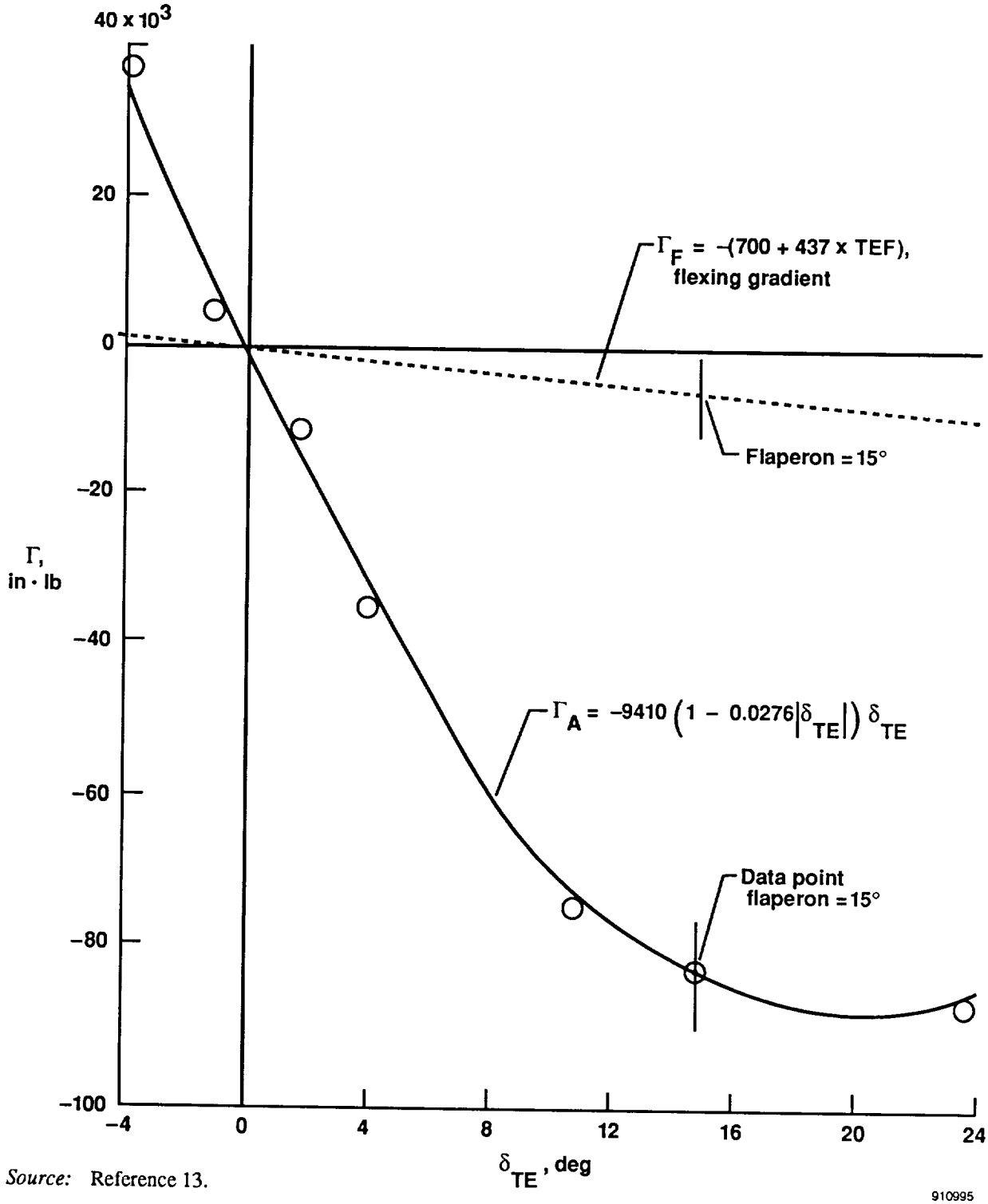

Source: Reference 13.

Figure 15. Outboard trailing-edge hinge moments caused by flexing and aerodynamic loading.

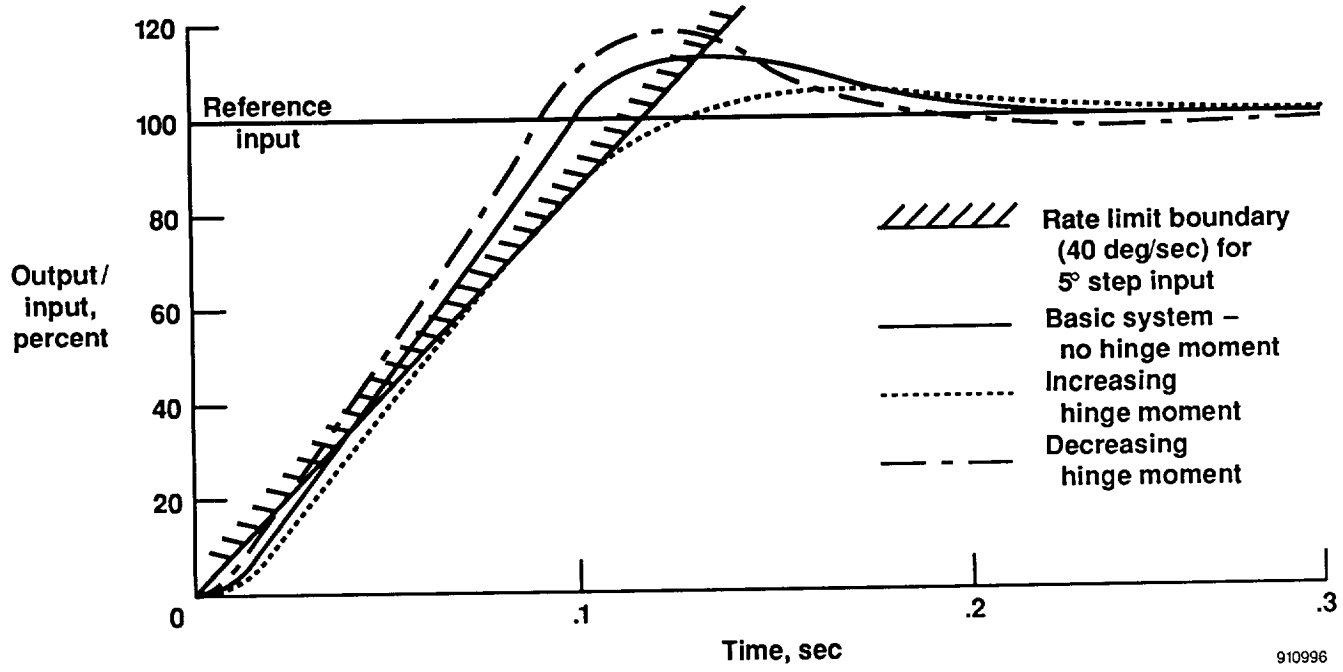

(a) Both power drive units operating at $K_T = 0.5$.

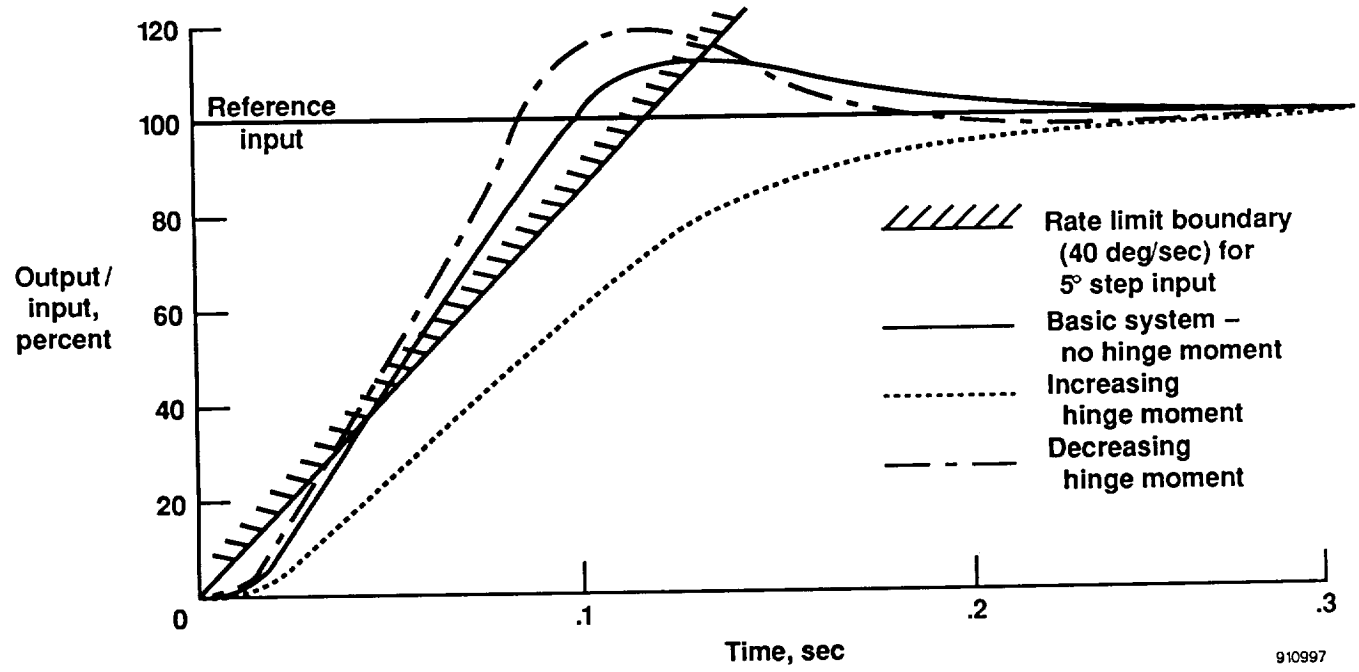

(b) One power drive unit operating at $K_T = 1.0$.

Figure 16. Calculated outboard flaperon response.

response, against the hinge moment $\sqrt{P_s - P_T} = 27$ results in a system that is almost critically damped. As before, rate limiting would also constrain the output response of both the single-PDU system aided by the hinge moment and the basic system with no hinge moment.

The MAW variable-cambered control surfaces can be closely approximated by a second-order system, where the roots are equated to the natural frequency and damping. Typically, the roots vary with gain. In most cases, the roots become more oscillatory and less damped as the closed-loop gain increases. The outboard servoactuator dynamic characteristics are summarized in figure 17, where the pressure gain is considered the independent variable. An opposing or downward input decreases the frequency and increases the damping ratio. For single-PDU operation, which doubles the torque load, the damping ratio approaches critical. In the upward commanded input, however, the aiding torque load causes the frequency to increase and the damping ratio to decrease.

OPERATIONAL PERFORMANCE

Hydraulic Pressure Variation With Control Activity

The greatest demands on the hydraulic systems occurred when the ME/GA mode was engaged and cycled continuously. This automode performs a dual task: to improve the airplane normal acceleration response from pilot commands and to reduce the vertical acceleration at the cockpit as a result of turbulence. Figure 18 shows a simplified block diagram of the ME/GA mode. With the mode engaged, the LE and TE of both wings were flexed symmetrically for direct lift control. The TE flaperons were flexed differentially for manual or augmented roll control. In addition, a cross-feed loop stabilon command was added to the basic CAS system to properly blend, phase, and obtain the desired vertical response of the A/C.

Moderate frequency sweeps were conducted in-flight to determine the variation in normal acceleration at the cockpit. The first sweep was performed with the basic CAS system at flight conditions of

$$\begin{aligned} M &= 0.75 \\ \bar{q} &= 325 \text{ lb/ft}^2 \\ \Lambda &= 26° \\ \text{LEF} &= 7° \\ \text{TEF} &= 9° \end{aligned}$$

to establish the peak-to-peak stabilon input, 5° peak-to-peak, over a frequency range of 0.3 to 2 Hz. At maximum control rate, the reduction in P_s of the primary and utility systems was slightly less than 100 lb/in^2. Then, the frequency sweep was repeated near the same flight conditions but with the ME/GA mode engaged at KMEGA = 0.4. The results of this test are shown in figure 19. The stabilon control activity, not shown, was approximately 5° peak-to-peak, and the TE camber varied approximately 3° peak-to-peak. The peak-to-peak change in the LE was less than 1°. At the maximum control rate of 2 Hz, the P_s for both systems was reduced to 2460 lb/in^2. At the conclusion of the sweep activity, the P_s recovered in typical exponential fashion. Approximately 2.4 sec were needed to recover from 2460 lb/in^2 to 90 percent of the maximum operating supply pressure $P_\infty = 3250$ lb/in^2. By fitting the constants from the experimental data, the following was derived:

$$P_s = P_\infty(1 - 0.243e^{t/-2.7}) \tag{14}$$

where

$$P_\infty = 3250 \text{ lb/in}^2 \tag{15}$$

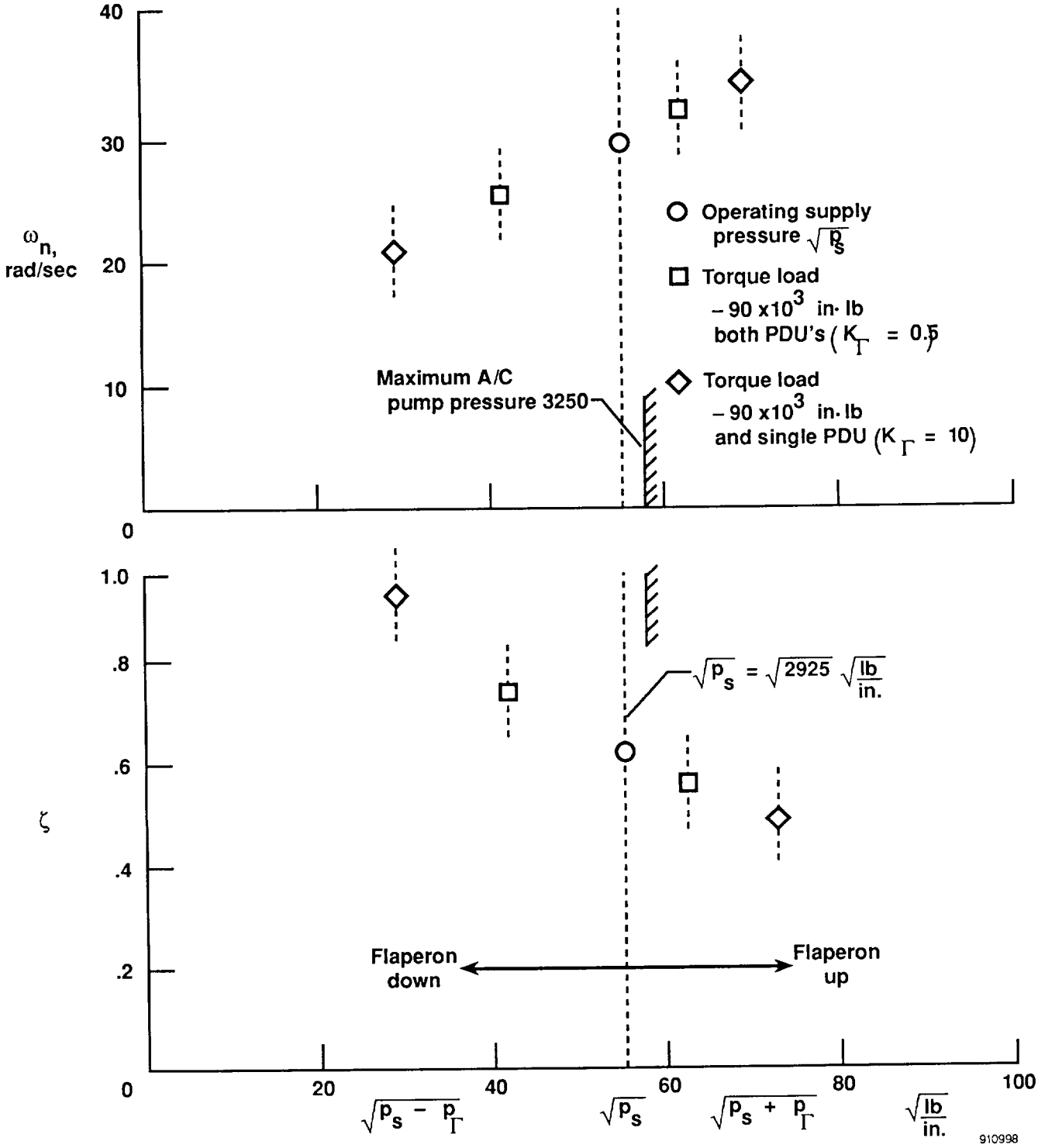

Figure 17. Summary of natural frequency and damping as a function of pressure gain.

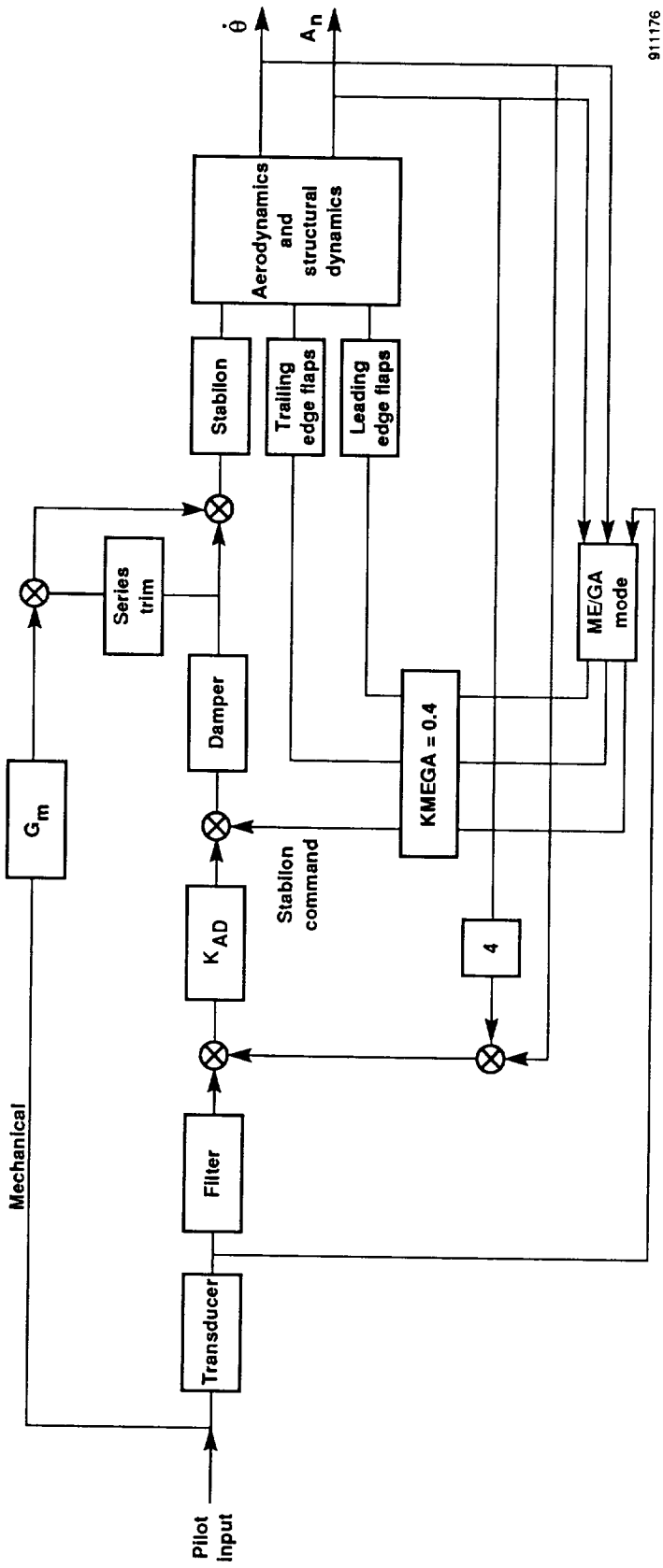

Figure 18. Block diagram of the AFTI/F-111 maneuver enhancement and gust alleviation control system.

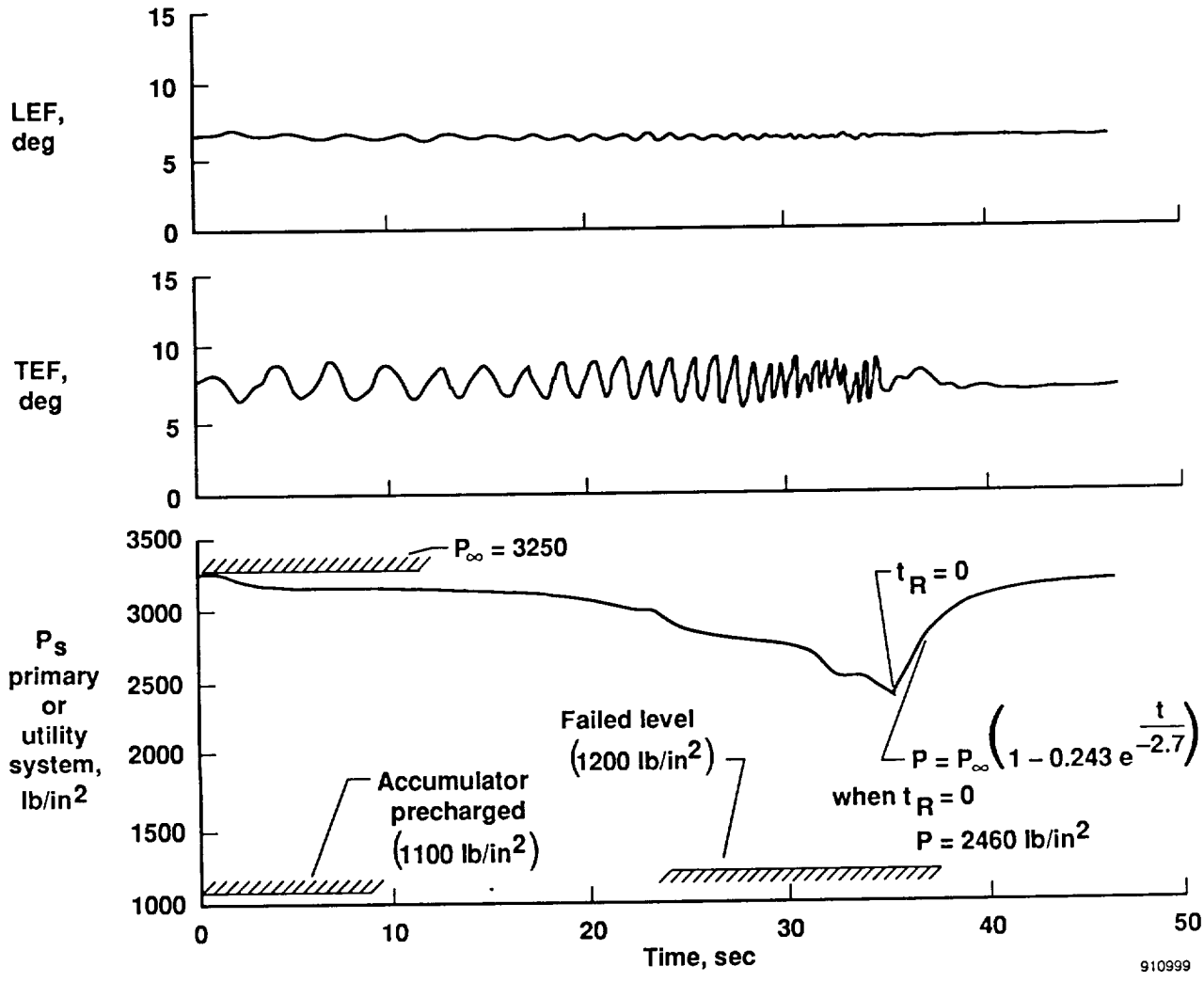

Figure 19. Primary or utility pressure reduction and recovery after a longitudinal frequency sweep.

At the recovery point,

$$t_R = 0$$
$$P_s = 2460 \text{ lb/in}^2 \tag{16}$$

The accumulator precharged pressure of 1100 lb/in^2 is indicated by the boundary. At 1200 lb/in^2, the primary system was programmed to default to the MAW backup mode.

Reliability and Dependability Assessment

The broad objectives of the phase 1 MAW program were to design, install, and flight test the variable-camber wing employing the MFCS. The MFCS operates in an isolated manner parallel to the existing F-111A CAS system so as not to affect the existing forward-loop control function of CAS. In addition, the overall design of the MFCS had to remain fully operational when the AFCS was added. These limitations permitted no modifications to the MAW servoelectronics and mechanical actuating systems (fig. 9). All automode systems, particularly those automodes that interfaced with the basic F-111A CAS, were required to be compatible with the MFCS and CAS.

The variable-cambered wings and MFCS computers were installed at DFRF. In November 1983, the fully installed systems were powered-up for the first time. Figure 20 shows the cumulative hours of ground and flight testing following a chronology of the various test events. During the initial checkout, 40 hr of operation were required to develop and affirm the sweep functions, to adjust the LVDT's, and to complete the functional checks of the MFCS computers and mechanical systems. The outlined preliminary and formal verification and validation (V&V) test procedures of the MFCS (ref. 9) required approximately 380 hr. The NASA qualification and acceptance testing, also part of the V&V commitment and the combined system testing, required less than 35 hr. Test results showed that MFCS computer modifications were necessary. A 5-mo delay in the program followed to change and update the computers and to complete the documentation reported in reference 14.

Retesting the computer modifications and developing a hangar preflight procedure required approximately 40 hr. Although the MAW control segments were in a static state during the loads calibrations, the MAW systems were operated for approximately 125 hr. The complete V&V testing, retesting of all functions, and testing of the basic F-111A system functions before the first flight required an additional 120 hr. In total, the MAW systems were operated 840 hr before flight. The first flight occurred October 18, 1985. Twenty-six flights completed the phase 1 MFCS program. During these 26 flights, 58 hr of flight time and an additional 250 hr of MAW systems ground operations accumulated.

Installation of the automode computers, ground and flight testing of the AFCS, and continued flight testing of the MFCS was accomplished during the second phase of the MAW program. A brief history, starting with the design requirements, the milestones, and a summary of the flight test results, is in reference 6.

The second phase began with the completion of flight 26. The first flight of the second phase, flight 27, occurred more than 9 mo later. During this period, the AFCS computers were installed, and the automode sensors and stabilon commands were calibrated. Following implementation of the automodes, the integrated MAW AFCS was functionally retested with a revised version of the V&V procedures (ref. 14). In addition, the hangar preflight procedures were changed to include the addition of the AFCS test sections. Before the AFCS was used in flight, ground resonance tests (GRT's) were conducted. These tests satisfied concerns about the ME/GA mode and its ability, through filters, to stabilize adequately the structural modes. The GRT's, with the ME/GA mode engaged, showed a lack of sufficient gain margin at the first wing body bending mode, 4 Hz, and the stabilon first symmetric bending mode, 12.8 Hz. Thus, the AFCS computers underwent modifications that required changing the filters and incorporating variable gains in the ME/GA mode feedback loops.

Between flights 26 and 27, the MAW system was ground tested for approximately 170 hr. Because of the computer modifications, flights 27, 28, and 29 were flown with only the MFCS. During flight 30, the more benign

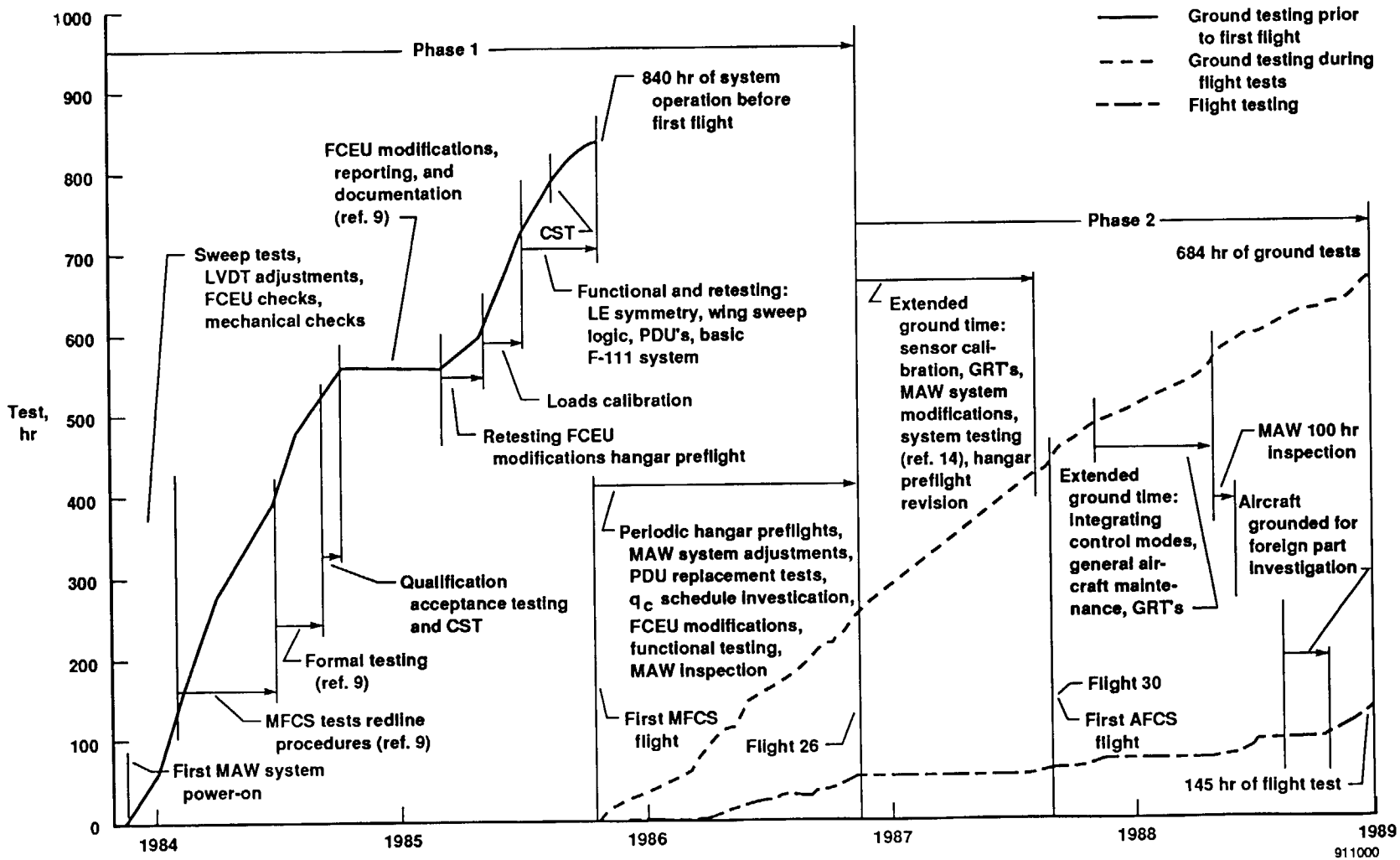

Figure 20. Accumulated hours of mission adaptive wing system testing.

automodes were engaged for the first time. Limited AFCS flight testing continued up through flight 35, and 70 hr of ground operation were added. The complete integration of the automodes, a second GRT to verify ME/GA mode stability, and a periodic inspection of the MAW system and aircraft added another 100 hr of ground system operation. In addition, routine tests and hangar preflights added approximately 84 hr of ground operation before the flight test program was completed. The last flight was flown in December 1988. A total of 145 hr of flight and 1524 hr of MAW system ground operation were accumulated. The 1669 combined hours represent the accumulated hours that the hydraulic systems were in operation. The control segments were operated sporadically and seldom cycled continuously; therefore, it is difficult, if not impossible, to estimate the total control cycles. In performing the primary lateral control function, however, the TE flaperons were undoubtedly cycled many times more than the LE and inboard flaps.

The variable-camber mechanism had a service life of 1000 hr as a design requirement (ref. 8). During the entire program, the 46 rotary actuators never failed nor was it necessary to replace a rotary actuator unit. The 16 PDU's did, however, require 37 component or full-assembly replacements. An account of the component or assembly replacements as compared with the accumulated hours of operation is shown in figure 21. The symbols in this figure show the component or assembly replaced and major failures. A sketch of a PDU is shown in figure 4. Most of the inital replacements or overhauls were caused by localized contamination that developed within the first 400 hr of system operation. Towards the end of the program, above 800 hr, leaks gradually developed around the motor shafts. Minute wetness was acceptable; however, if collectable drops were present under pressure conditions, the motor seals were replaced. During the last 250 hr of operation, no component or unit replacements were necessary. The six major failures would have downmoded the systems to at least backup and would have required single-PDU operation or, perhaps, the affected segment would have required braking. All six major failures occurred on the ground. No major failures occurred during the last 700 hr of operation. Most important, there were no in-flight failures, as previously reported in reference 6.

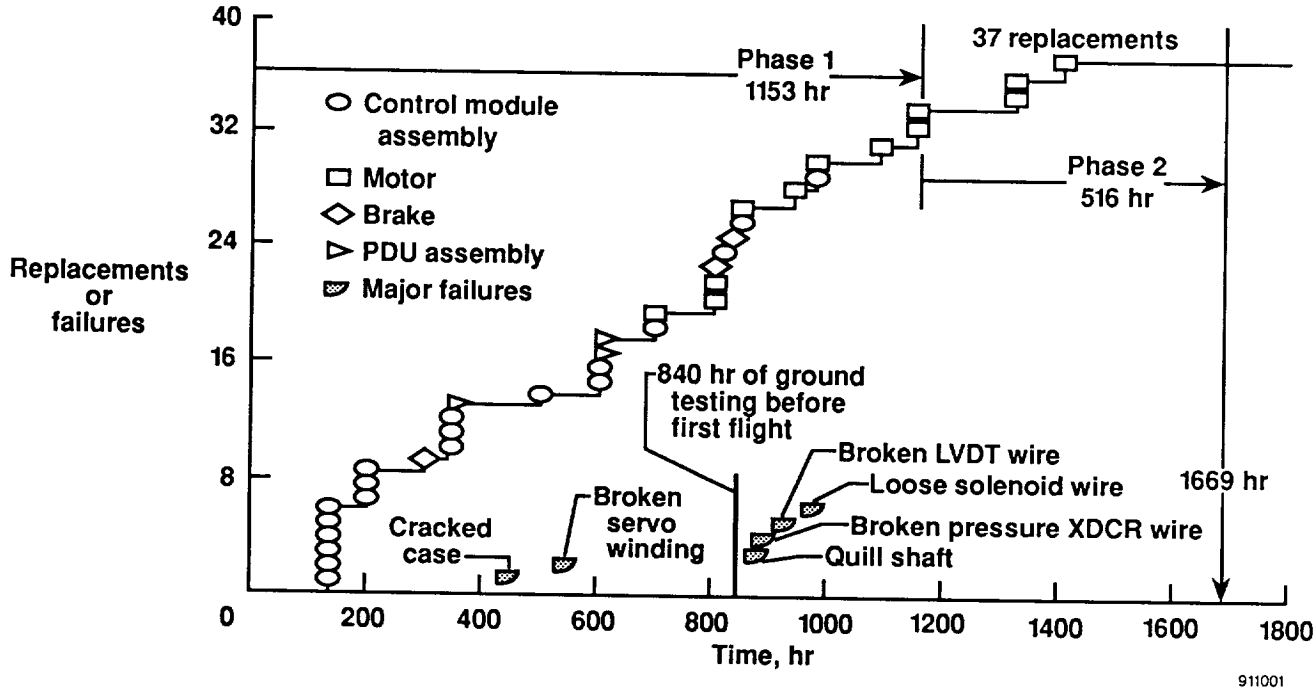

Figure 21. Dependability assessment of the power drive units and components as a function of hours of operation.

CONCLUSIONS

The advanced fighter technology integration aircraft, a preproduction F-111A aircraft, was fitted with a smooth variable-camber mission adaptive wing. Sixteen power drive units and 46 rotary actuators produced active variable-camber control. During the entire phase 1 and 2 program, 1524 hours of ground testing and 145 hours of flight testing were accumulated with the mission adaptive wing servoactuator mechanisms operating. Analytical predictions were acquired to complement the measure frequency responses.

The following conclusions were reached from the ground tests, flight tests, and analytical predictions:

1. The mission adaptive wing system servoactuator mechanisms exceeded the 1000-hours service life requirement by 67 percent.
2. There were no rotary actuator failures or replacements.
3. Error signal and pressure equalization loops were effective in minimizing force fights.
4. During an in-flight frequency sweep with the maneuver enhancement and gust alleviation automode engaged, the mission adaptive wing hydraulic system showed adequate flow capability and recover response.
5. The analytical linear calculations of the closed-loop servoactuator model matched the measured amplitude ratio. The phase angle was acceptable for up to twice the natural frequency.
6. Successful primary and backup control was provided by the mission adaptive wing systems with no in-flight failures during the flight tests.
7. During ground operation, 37 power drive unit components or full-assembly replacements were necessary, and 6 major failures that would have downmoded the systems to backup occurred.
8. There were no major failures during the last 700 hours of operation. In addition, no component or unit replacements were necessary during the last 250 hours of operation.

APPENDIX
NOMENCLATURE

Abbreviations

A/C	aircraft
AFCS	automatic flight control system
AFTI	advanced fighter technology integration
AR	amplitude ratio, deg/deg
BL	butt line, in.
CAS	command augmentation system
Ch	channel
CID	in^3 in displacement
CST	combined system tests
DAC	digital to analog
Demod	demodulated
DFRF	Dryden Flight Research Facility
FCEU	flight control electronic unit
FLT	flight
FS	fuselage station, in.
GRT	ground resonance test
KMEGA	ME/GA mode gain
LE	leading edge
LEF	leading-edge flap, deg
Lim	limiter
LVDT	linear voltage differential transformer
MAC	mean aerodynamic chord
MAW	mission adaptive wing
ME/GA	maneuver enhancement and gust alleviation
MFCS	manual flight control system
PDU	power drive unit
RV	relief valve
TACT	transonic aircraft technology
TE	trailing edge
TEF	trailing-edge flap, deg
V	volts
Vdc	volts direct current
V&V	verification and validation

Letter and Mathematical Symbols

A	area, in^2
A_n	normal acceleration near the cockpit, g
C	control variable
D_m	motor displacement, in^3/rad
e	natural logarithm base
F_N	net force due to pressure element area, lb
F_Γ	generalized force due to torque, lb
G_m	stick to stabilon mechanical gearing, basic F-111A aircraft, deg/in.
H_P	aircraft primary hydraulics
H_U	aircraft utility hydraulics
K_A	actuator loop gain
K_{AD}	adaptive gain, sec
K_D	value drive amplifier gain, mA/Vdc
K_e	equivalent system gain, $(K_A \times 57.3 \times 0.77)$, Vdc/rad
K_F	feedback filter transfer function
K_P	pressure equalization gain, V
K_Q	flow gain, $in^4/\sqrt{lb}$-in-sec
K_{sv}	servovalue gain, in/mA
K_Γ	torque moment gain, both PDU's operating $K_\Gamma = 0.5$; single PDU, $K_\Gamma = 1.0$
M	Mach number
m	mass
mA	milliampere
P	pressure, lb/in^2
P_R	return pressure, $P_R \Rightarrow 0$, lb/in^2
P_s	supply pressure, lb/in^2
$\sqrt{P_s \pm P_\Gamma}$	pressure gain, $\sqrt{lb}/in$
P_Γ	pressure due to torque moment feedback, lb/in^2
P_∞	maximum supply pressure, lb/in^2
p_n	PDU pressure sensors
Q	rate of flow, in^3/sec
q_c	impact pressure, lb/ft^2
$\bar{q}$	dynamic pressure, lb/ft^2
R	control reference
s	Laplace transform
t	time, sec
t_R	initial recovery point, sec

X_V	valve position, in.
Γ	torque moment, in-lb
Γ_A	aerodynamic hinge-moment, in-lb
Γ_F	flexing torque moment, in-lb
Γ_T	total torque moment, in-lb
Δ	small change
δ_C	small change in commanded position, deg
δ_F	small change in flap position, deg
δ_{TE}	small change in trailing-edge position, deg
ε	error signal, V
η_t, η'_t	gear ratios; actuator $\rightarrow$ motor, surface $\rightarrow$ actuator
$\dot{\theta}$	pitch rate, deg/sec
Λ	wing sweep, deg
ς	damping ratio
τ	time constants, sec
τ_F	filter time constant, sec
τ_D	valve drive amplifier time constant, sec
τ_{SV}	servovalve time constant, sec
ω	frequency, rad/sec
ω_n	natural frequency, rad/sec
$\propto$	varies as
$\|\|$	absolute value
ϕ	phase angle, deg

REFERENCES

1. *Symposium on Transonic Aircraft Technology (TACT)*, AFFDL-TR-78-100, Lancaster, California, August 15–17, 1978.
2. Larson, Richard R., *AFTI/F-111 MAW Flight Control System and Redundancy Management Description*, NASA TM 88267, 1987.
3. Hall, Joseph M., *AFTI/F-111 Flight Control System*, AFWAL-TR-87-3012, March 3, 1988.
4. Hall, Joseph M., *Executive Summary: AFTI/F-111 Mission Adaptive Wing*, WRDC-TR-89-3083, September 1989.
5. Bussing, Paul R., et al. *AFTI/F-111 Flight Test Design Substantiation Final Report*, WRDC-TR-89-3084, September 1989.
6. *Advanced Fighter Technology Integration F-111 Mission Adaptive Wing*, NASA CP 3055, 1990.
7. Martin, C.E., *Final Flight Control Subsystem Engineering Report for the F-111A Aircraft*, FZM-12-13468, General Dynamics Corporation, Fort Worth, Texas, March 1980.
8. Statkus, Frank D., *AFTI/F-111 Structures/Mechanical Systems*, AFWA-TR-87-3036, July 1987.
9. Rustik, J.J. and AFTI Engineering, *AFTI/F-111 MAW Flight Control System Test Procedures WBS 13000*, 0365-10060-2, Revision D, The Boeing Company, Seattle, Washington, June 1985.
10. White, D.K., *F-111 Hydraulic System Design Report: AF33(657)-8260*, FZM-12-947A, General Dynamics Corporation, Fort Worth, Texas, April 1969.
11. Hynes, R.J., *AFTI/F-111 MAW Manual Flight Control System Description*, D365-10100-1, The Boeing Company, Seattle, Washington, December 1983.
12. Larson, Richard R., "Flight Control System Development and Flight Test Experience with the F-111 Mission Adaptive Wing Aircraft," in *AIAA Guidance, Navigation and Control Conference*, Williamsburg, Virginia, August 18–20, 1986, pp. 784-801.
13. Hall, Joseph M., *AFTI/F-111 MAW Flight Simulator Description*, D365-10057-1, The Boeing Company, Seattle, Washington, September 23, 1981.
14. Hynes, Robert J. and AFCS Engineering (L-8943), *AFCS MAW Flight Control System Test Procedures for the Automatic System*, D365-10060-14, The Boeing Company, Seattle, Washington, October 23, 1986.

REPORT DOCUMENTATION PAGE

Form Approved
OMB No. 0704-0188

Public reporting burden for this collection of information is estimated to average 1 hour per response, including the time for reviewing instructions, searching existing data sources, gathering and maintaining the data needed, and completing and reviewing the collection of information. Send comments regarding this burden estimate or any other aspect of this collection of information, including suggestions for reducing this burden, to Washington Headquarters Services, Directorate for information Operations and Reports, 1215 Jefferson Davis Highway, Suite 1204, Arlington, VA 22202-4302, and to the Office of Management and Budget, Paperwork Reduction Project (0704-0188), Washington, DC 20503.

1. AGENCY USE ONLY *(Leave blank)*	2. REPORT DATE	3. REPORT TYPE AND DATES COVERED
	April 1992	Technical Memorandum

4. TITLE AND SUBTITLE

Variable-Camber Systems Integration and Operational Performance of the AFTI/F-111 Mission Adaptive Wing

5. FUNDING NUMBERS

WU-533-02

6. AUTHOR(S)

John W. Smith, Wilton P. Lock, and Gordon A. Payne

7. PERFORMING ORGANIZATION NAME(S) AND ADDRESS(ES)

NASA Dryden Flight Research Facility
P.O. Box 273
Edwards, CA 93523-0273

8. PERFORMING ORGANIZATION REPORT NUMBER

H-1748

9. SPONSORING/MONITORING AGENCY NAME(S) AND ADDRESS(ES)

National Aeronautics and Space Administration
Washington, DC 20546-0001

10. SPONSORING/MONITORING AGENCY REPORT NUMBER

NASA TM-4370

11. SUPPLEMENTARY NOTES

John W. Smith: PRC Inc., Edwards, California
Wilton P. Lock and Gordon A. Payne: Dryden Flight Research Facility, Edwards, California

12a. DISTRIBUTION/AVAILABILITY STATEMENT

Unclassified — Unlimited
Subject Category 08

12b. DISTRIBUTION CODE

13. ABSTRACT ***(Maximum 200 words)***

The advanced fighter technology integration, the AFTI/F-111 aircraft, is a preproduction F-111A testbed research airplane that was fitted with a smooth variable-camber mission adaptive wing. The camber was positioned and controlled by flexing the upper skins through rotary actuators and linkages driven by power drive units. This report describes the wing camber and control systems. The measured servoactuator frequency responses are presented along with analytical predictions derived from the integrated characteristics of the control elements. A mission adaptive wing system chronology is used to illustrate and assess the reliability and dependability of the servoactuator systems during 1524 hours of ground tests and 145 hours of flight testing.

14. SUBJECT TERMS

Advanced fighter technology integration; Flight control; Hydraulic systems; Servoactuators; Variable-camber

15. NUMBER OF PAGES

44

16. PRICE CODE

A03

17. SECURITY CLASSIFICATION OF REPORT	18. SECURITY CLASSIFICATION OF THIS PAGE	19. SECURITY CLASSIFICATION OF ABSTRACT	20. LIMITATION OF ABSTRACT
Unclassified	Unclassified	Unclassified	Unlimited

NSN 7540-01-280-5500

Standard Form 298 (Rev. 2-89)
Prescribed by ANSI Std. Z39-18
298-102

NASA-Langley, 1992